Variation Based Dense 3D Reconstruction Using Photometric Invariants from Monocular Mini-Laparoscopic Sequences

Additional Material: Figures

Sven Painer

Contents

List of Figures

Chapter 1

Introduction

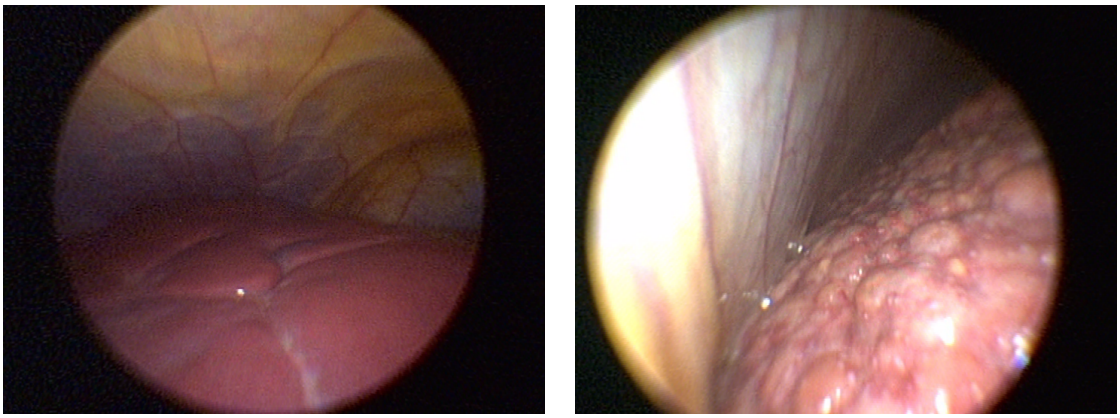

(a) Scarred liver (b) Liver cirrhosis

Figure 1.1: Two examples of mini-laparoscopic images. (a) shows a scarred liver surface and (b) shows a liver surface with severe cirrhosis. These images are taken from real mini-laparoscopic sequences by courtesy of Universitätsklinikum Hamburg-Eppendorf (UKE).

Chapter 2

Theoretical Background

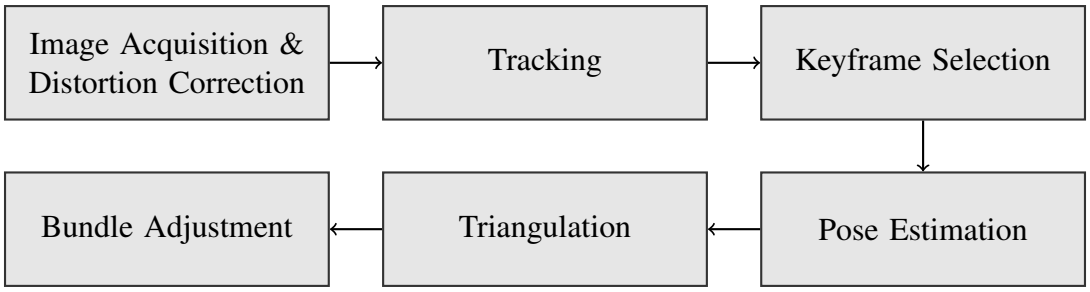

Figure 2.1: Overview of the sparse reconstruction. The necessary steps for the Structure from Motion approach are shown.

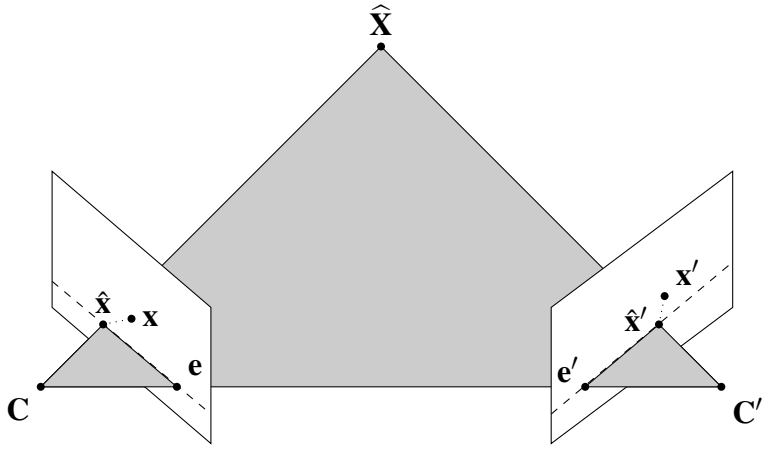

Figure 2.2: Overview of the epipolar geometry. The camera centers are located at $\mathbf{C}$ and $\mathbf{C}'$ and the epipoles are denoted by $\mathbf{e}$ and $\mathbf{e}'$. The 3D point $\widehat{\mathbf{X}}$ is projected into both images onto the points $\hat{\mathbf{x}}$ and $\hat{\mathbf{x}}'$, respectively. These could be shifted to $\mathbf{x}$ and $\mathbf{x}'$ due to noise. In both image planes the epipolar lines are given by a dashed line.

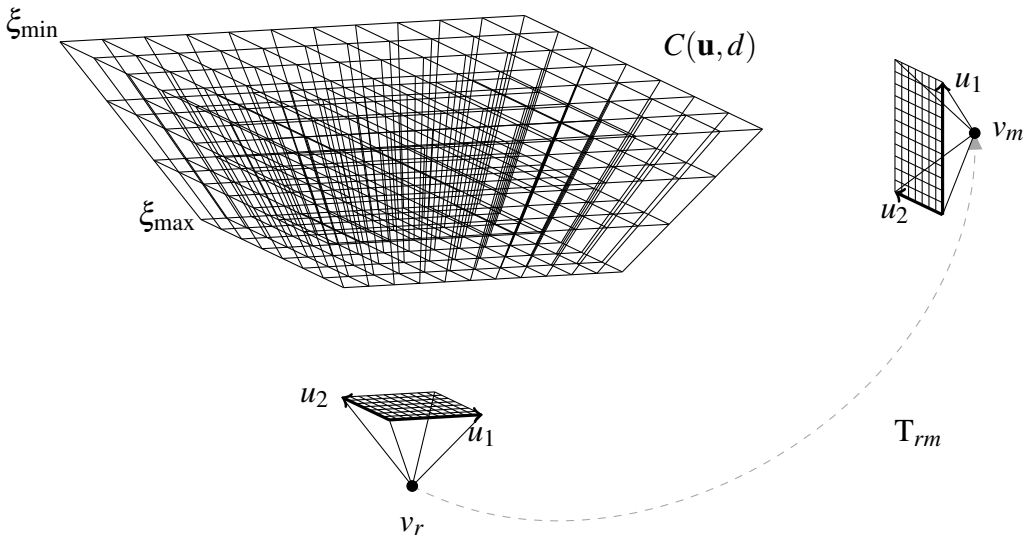

Figure 2.3: Illustration of the procedure to compute the cost volume. All pixels of the reference frame v_r are backprojected into the 3D space for all depth samples d between ξ_{min} and ξ_{max}. In this example, there are three depth samples. This voxel volume is then projected into another frame v_m. The values of the pixel in the reference frame and the pixel in the other frame are then taken to compute the cost volume. This figure is taken from [1].

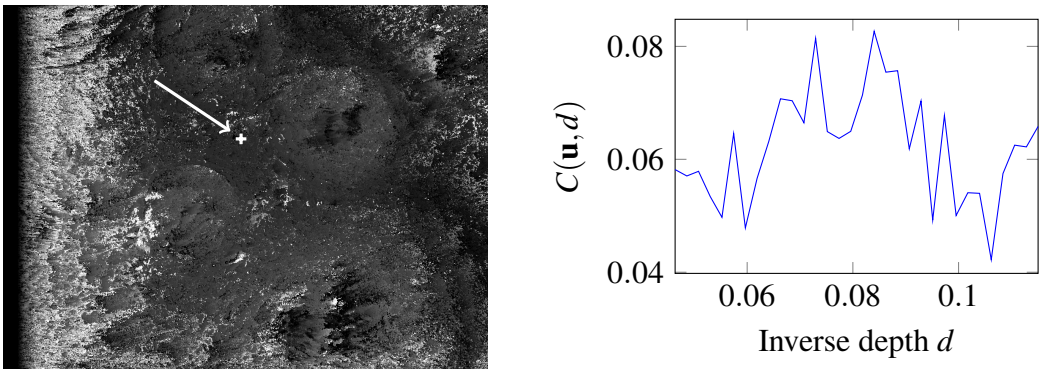

(a) Inverse depth map (b) Photometric error for the marked pixel $\mathbf{u}$

Figure 2.4: Inverse depth map constructed from cost volume. (a) shows an inverse depth map constructed only by the cost volume. For each pixel, the inverse depth value with the minimum costs is taken. (b) shows the error function for the pixel $\mathbf{u}$ that is marked in (a).

Chapter 3

Implementation

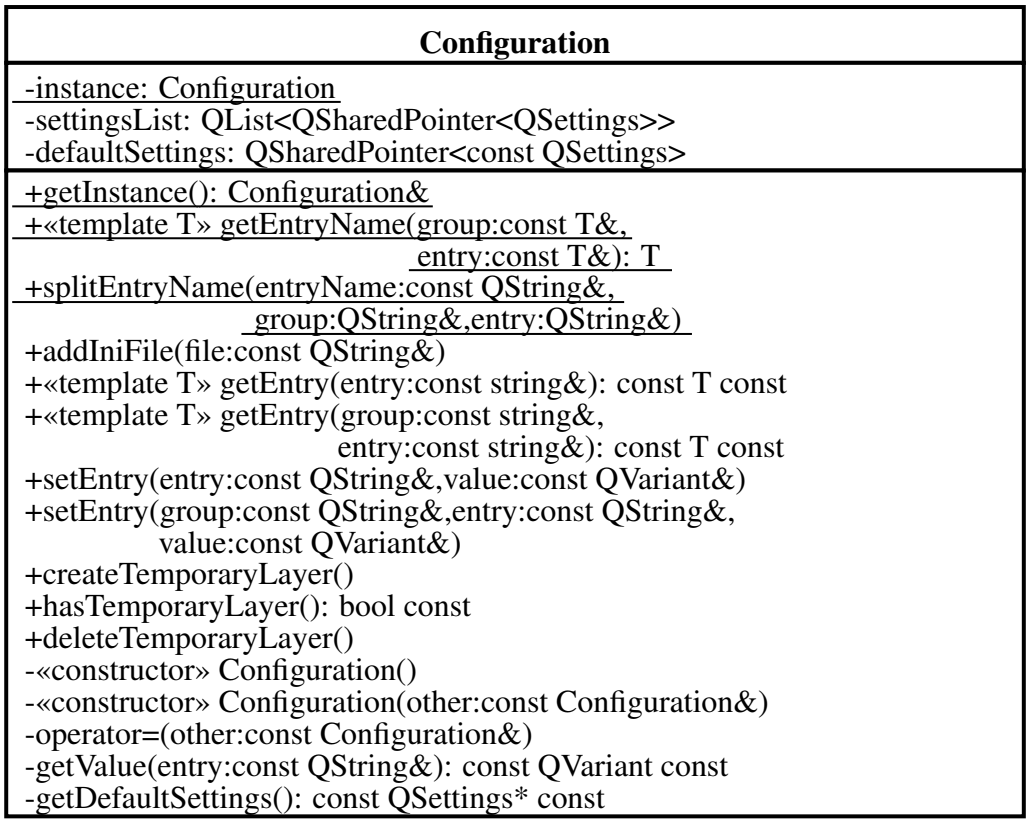

Figure 3.1: Class diagram of the class *Configuration*.

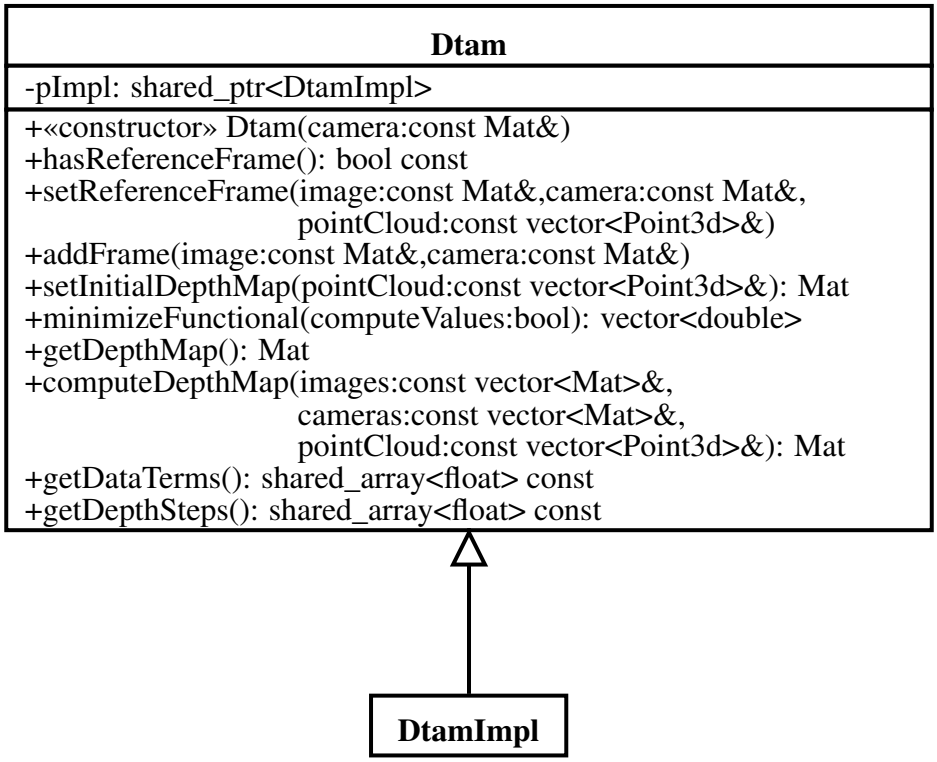

Figure 3.2: Class diagram of the dense reconstruction. Only the public interface of the class *Dtam* is shown.

Chapter 4

Evaluation

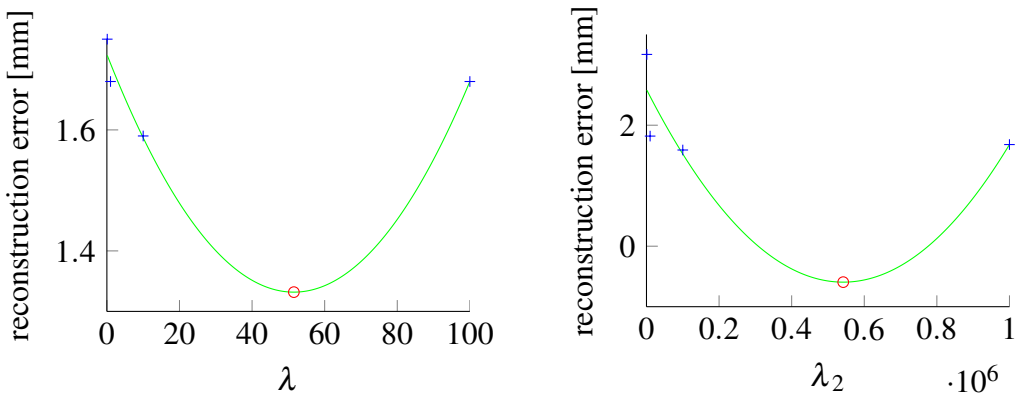

Figure 4.1: Estimation of dense reconstruction parameters. The dense reconstruction is executed with different parameter values. The crosses indicate these measurements. The line shows a parabola that is estimated to fit the data. The circle marks the minimum of this parabola that is also taken as the parameter value.

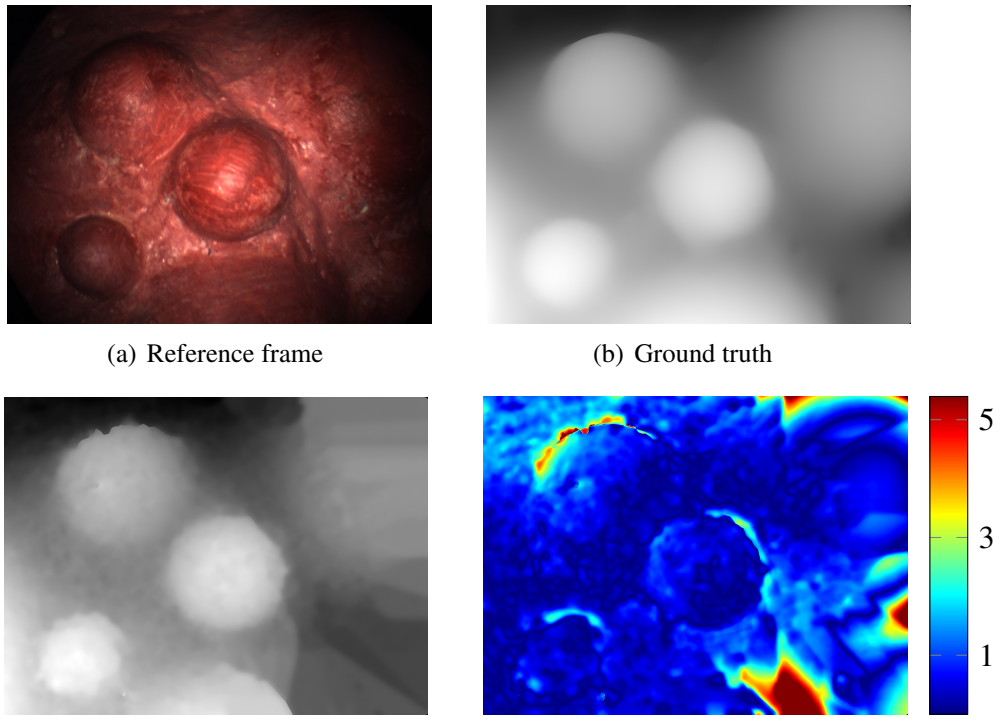

(a) Reference frame (b) Ground truth

(c) Reconstruction (d) Error [mm]

Figure 4.2: Example of a reconstructed frame. (a) shows the reference frame. (b) shows the ground truth inverse depth map and (c) shows the reconstructed inverse depth map. The error for each pixel in millimeters is illustrated in (d).

Appendix A

Class Diagrams of CUDA Framework

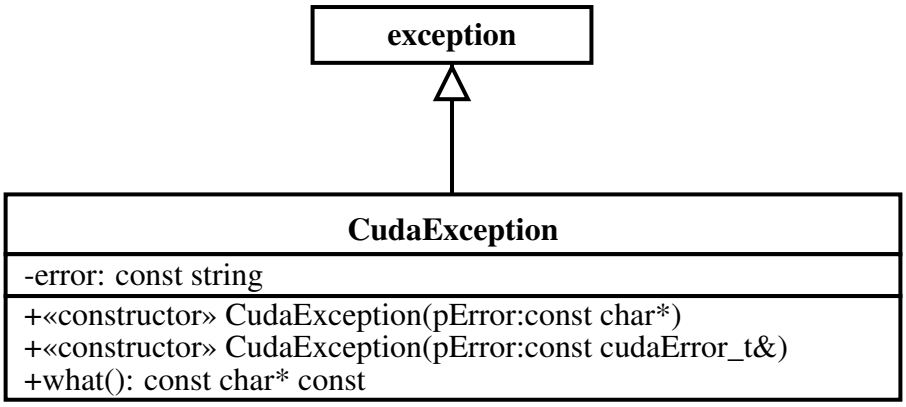

Figure A.1: Class diagram of the class *CudaException*.

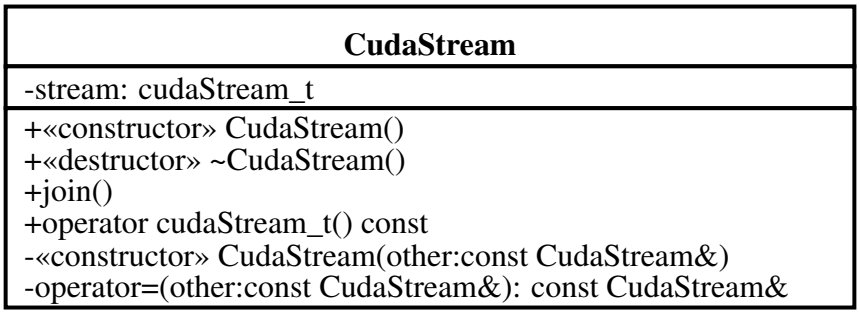

Figure A.2: Class diagram of the class *CudaStream*.

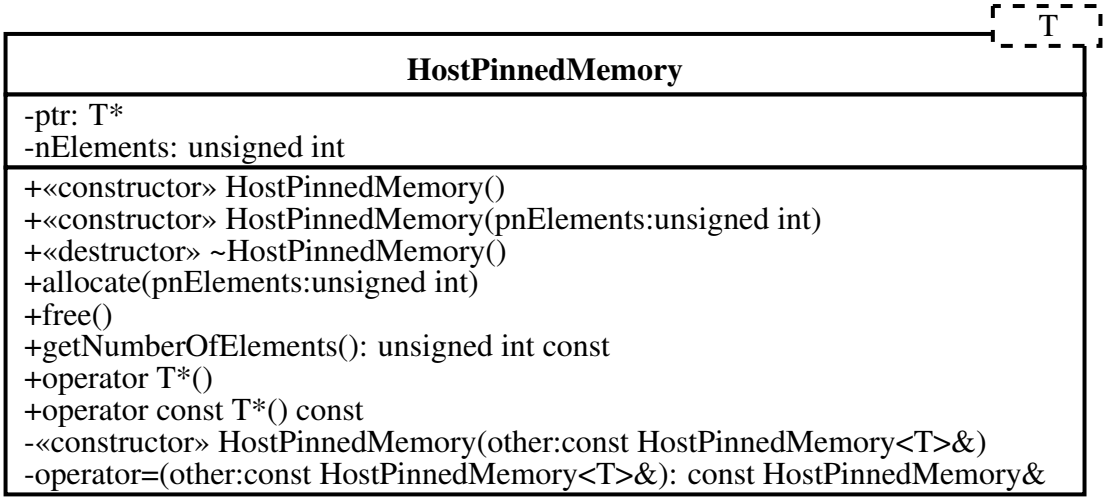

Figure A.3: Class diagram of the class *HostPinnedMemory*.

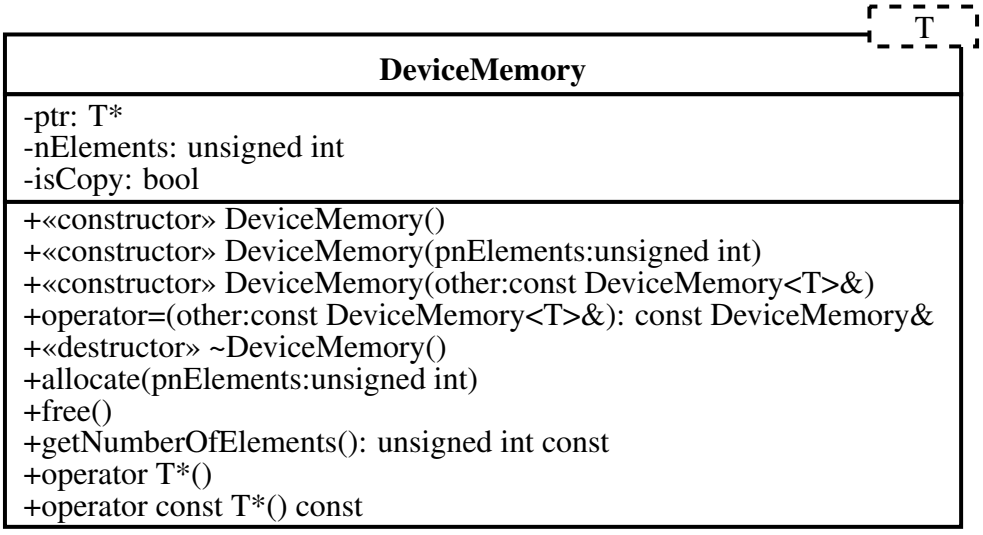

Figure A.4: Class diagram of the class *DeviceMemory*.

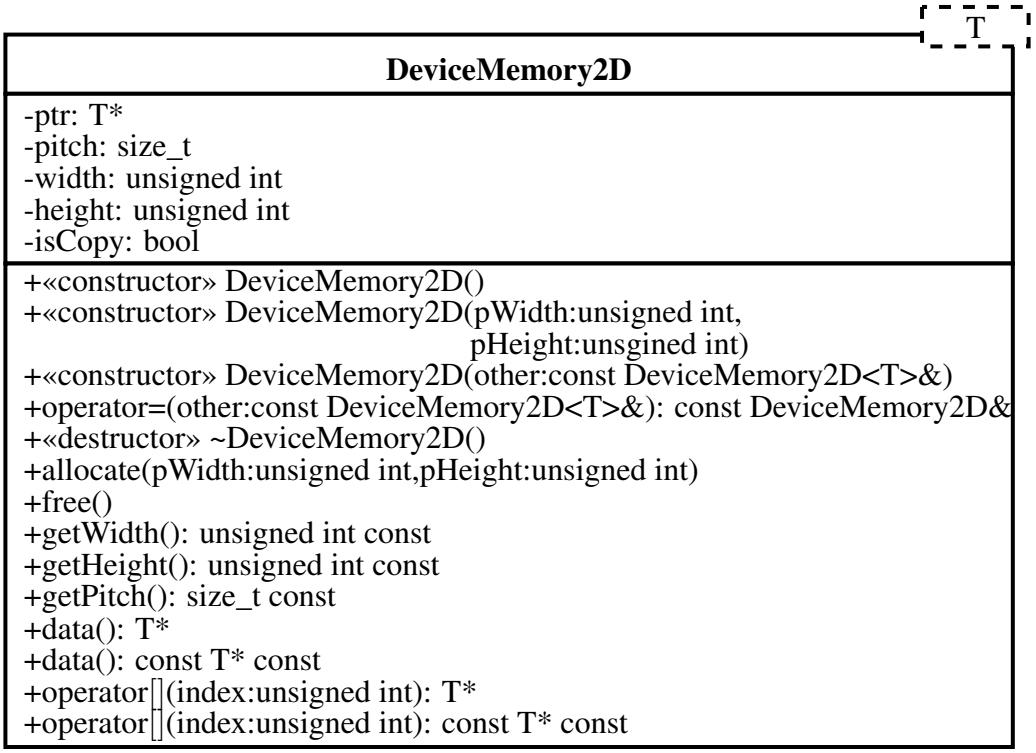

Figure A.5: Class diagram of the class *DeviceMemory2D*.

Appendix B

Class Diagrams of Sparse Reconstruction

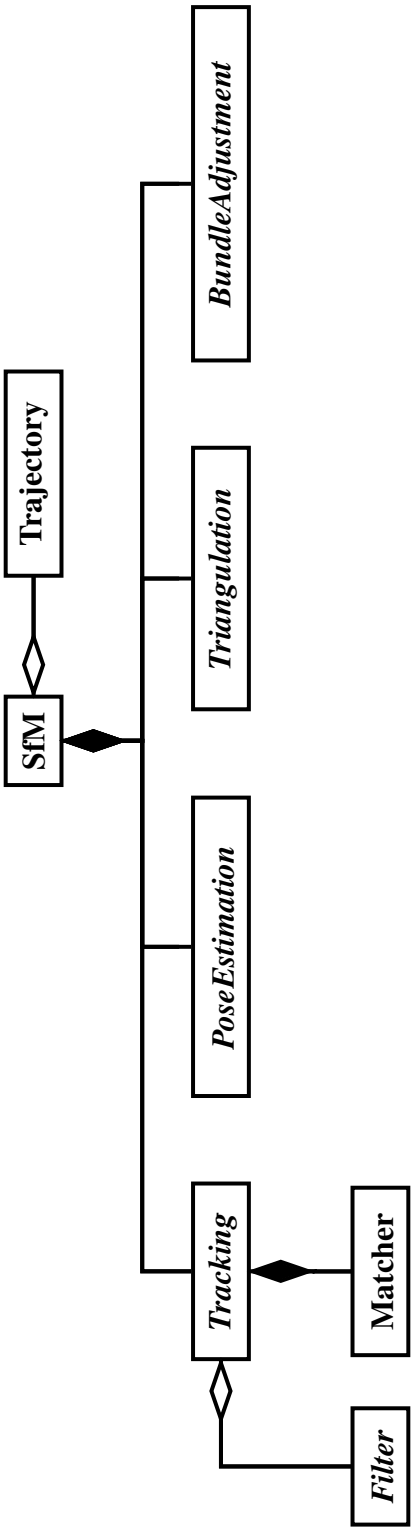

Figure B.1: Overview of the classes used in the sparse reconstruction. The reconstruction steps are implemented by using the strategy pattern. Only the base classes of the strategies are shown.

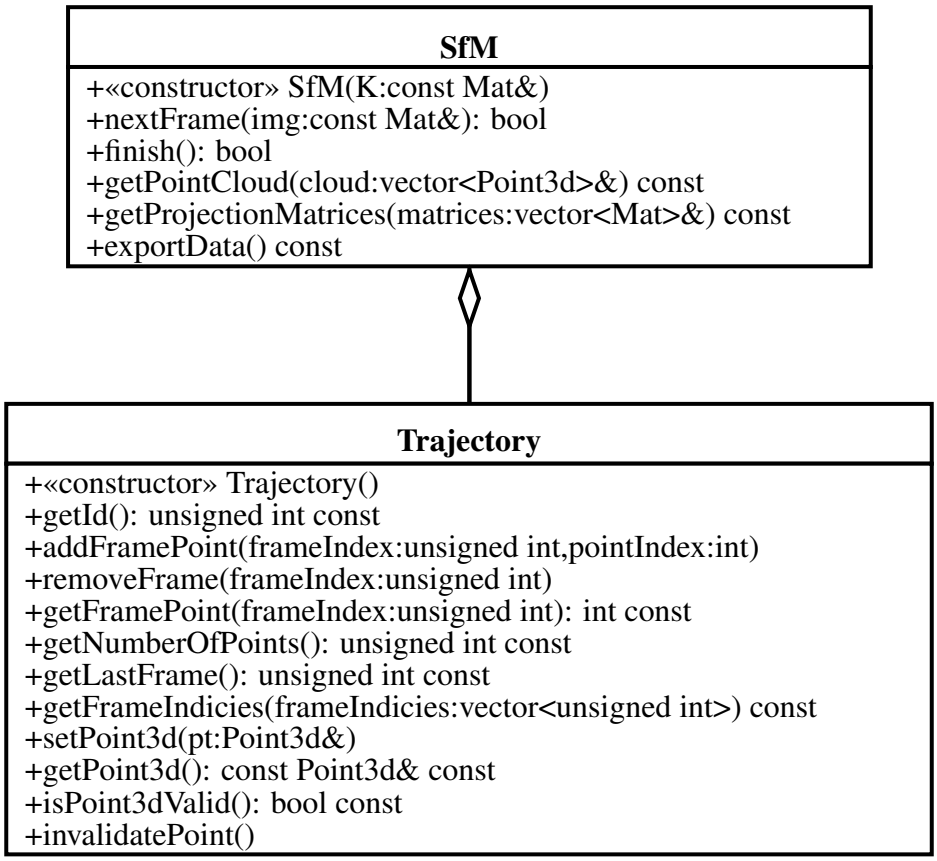

Figure B.2: Class diagram of the classes *SfM* and *Trajectory*. Only the public interface is shown.

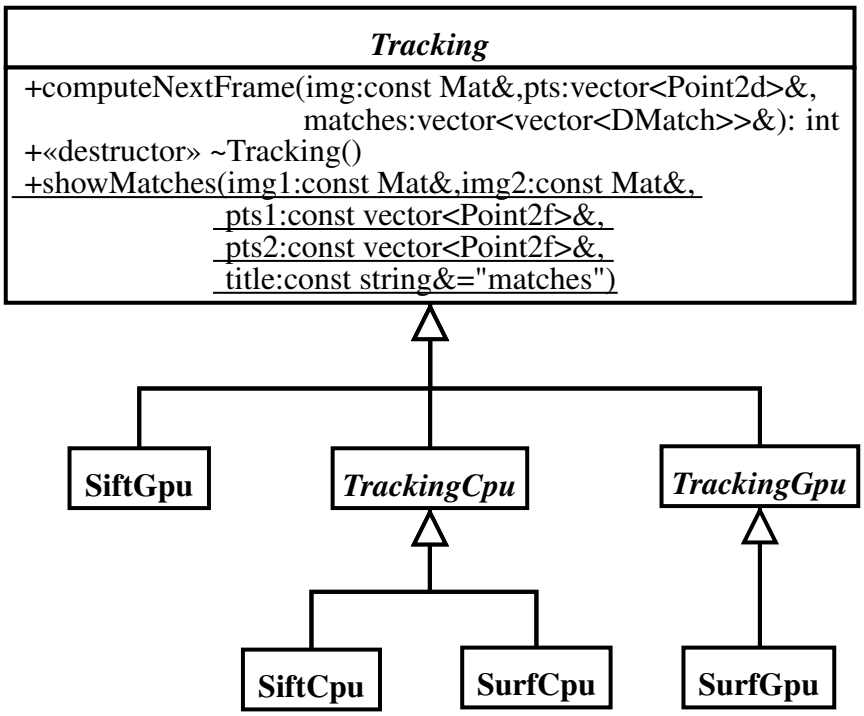

Figure B.3: Class diagram of the classes belonging to the tracking strategy. Only the public interface of the class *Tracking* is shown.

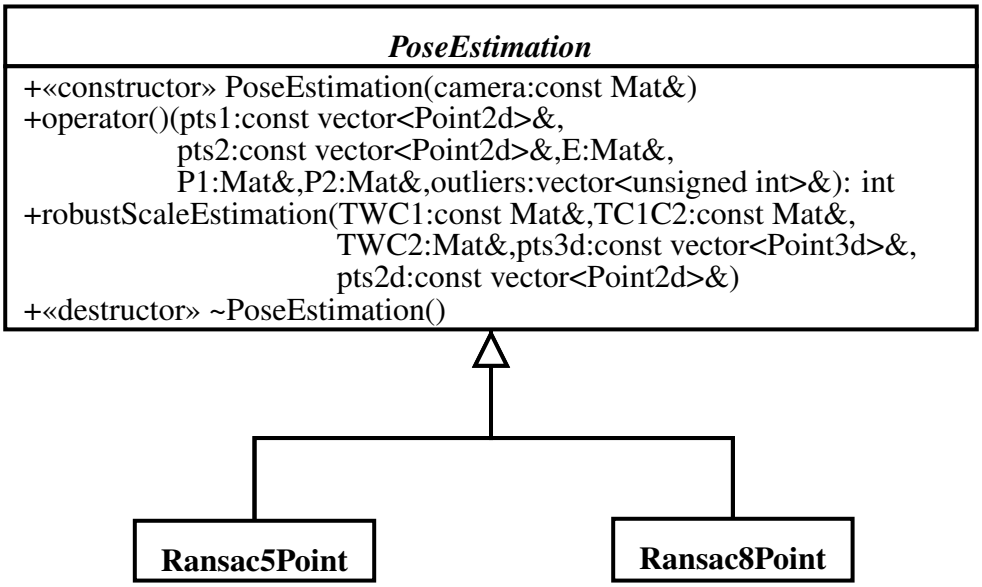

Figure B.4: Class diagram of the classes belonging to the pose estimation strategy. Only the public interface of the class *PoseEstimation* is shown.

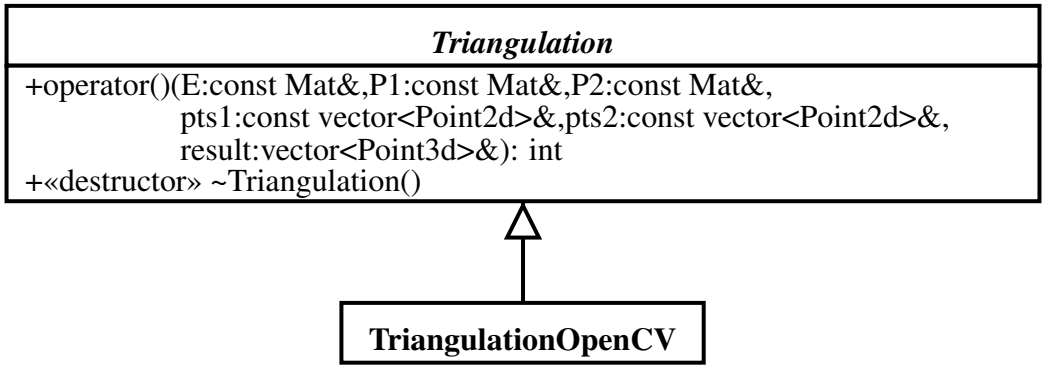

Figure B.5: Class diagram of the classes belonging to the triangulation strategy. Only the public interface of the class *Triangulation* is shown.

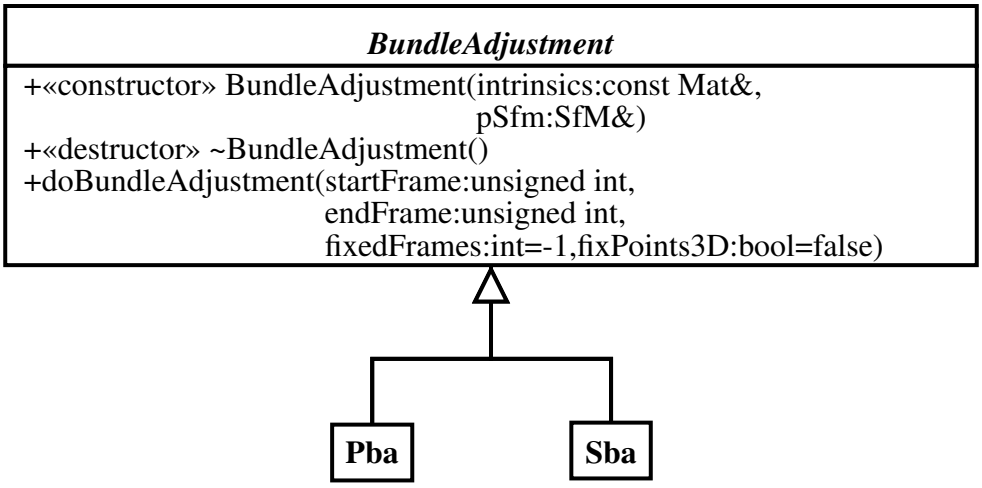

Figure B.6: Class diagram of the classes belonging to the bundle adjustment strategy. Only the public interface of the class *BundleAdjustment* is shown.

Appendix C

Evaluation Results of Sparse Reconstruction

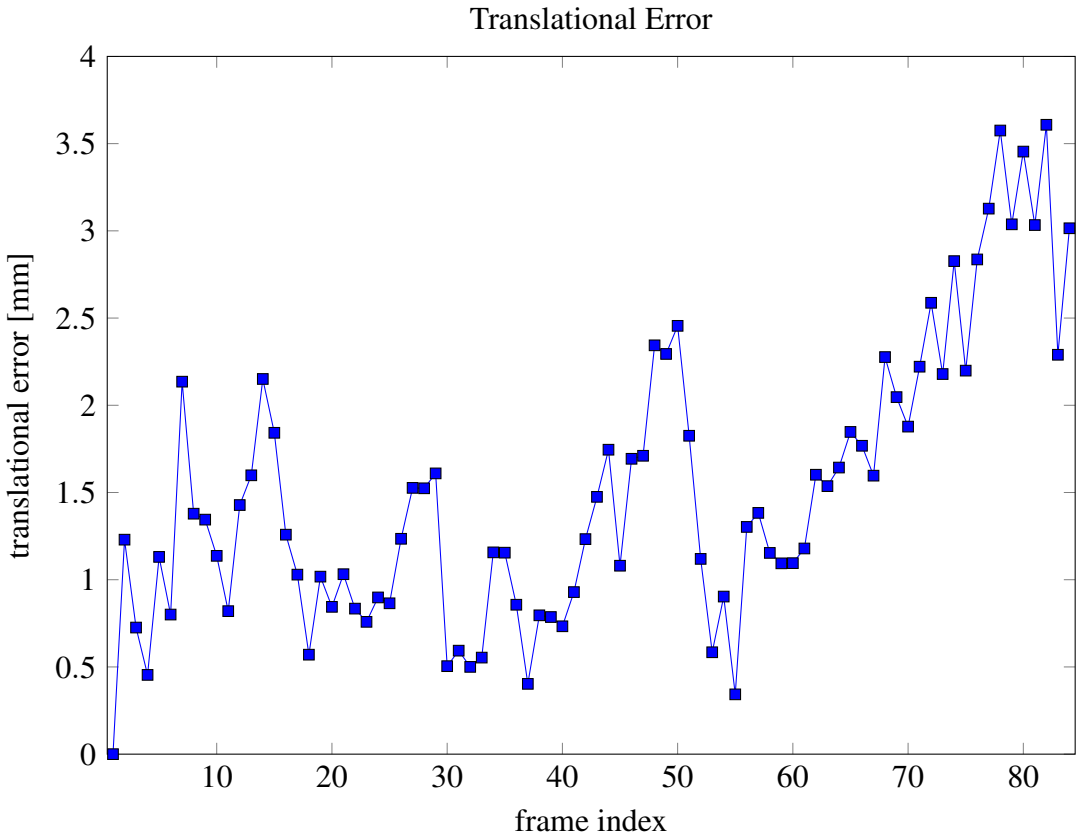
Translational Error
translational error [mm]
frame index
0
0.5
1
1.5
2
2.5
3
3.5
4
10
20
30
40
50
60
70
80

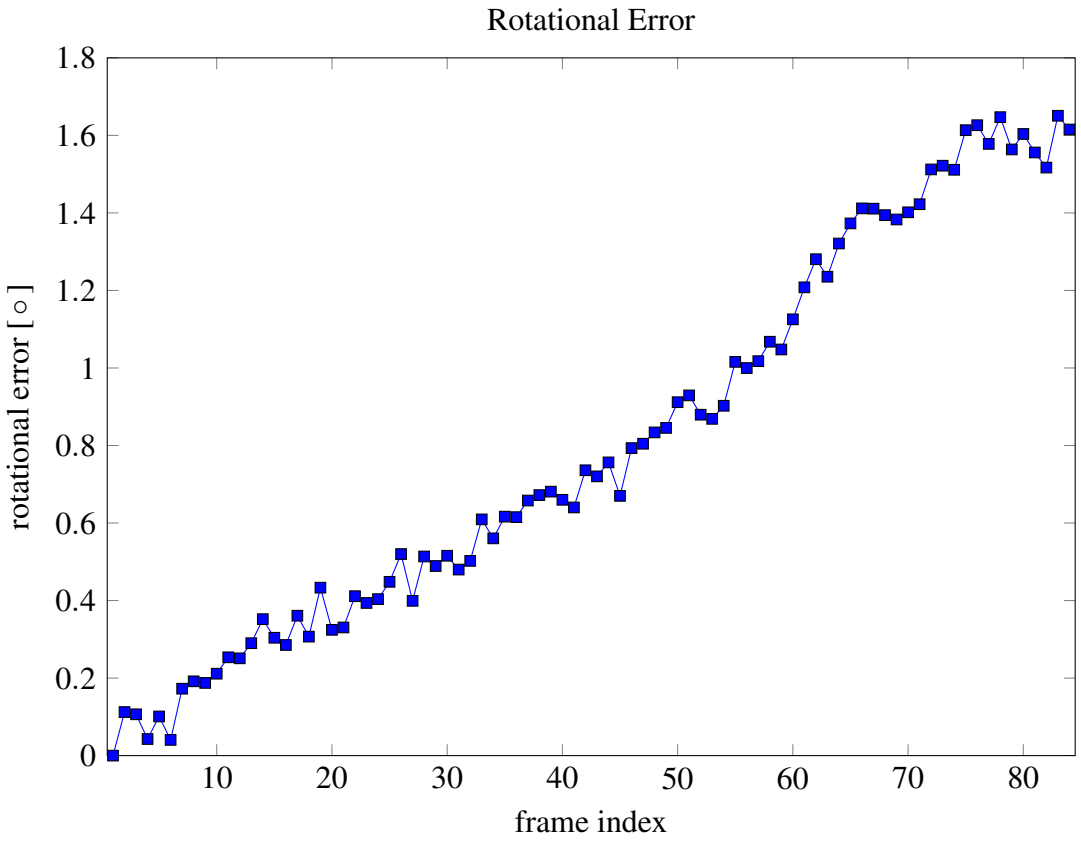
Rotational Error
rotational error [∘]
frame index
0
0.2
0.4
0.6
0.8
1
1.2
1.4
1.6
1.8
10
20
30
40
50
60
70
80

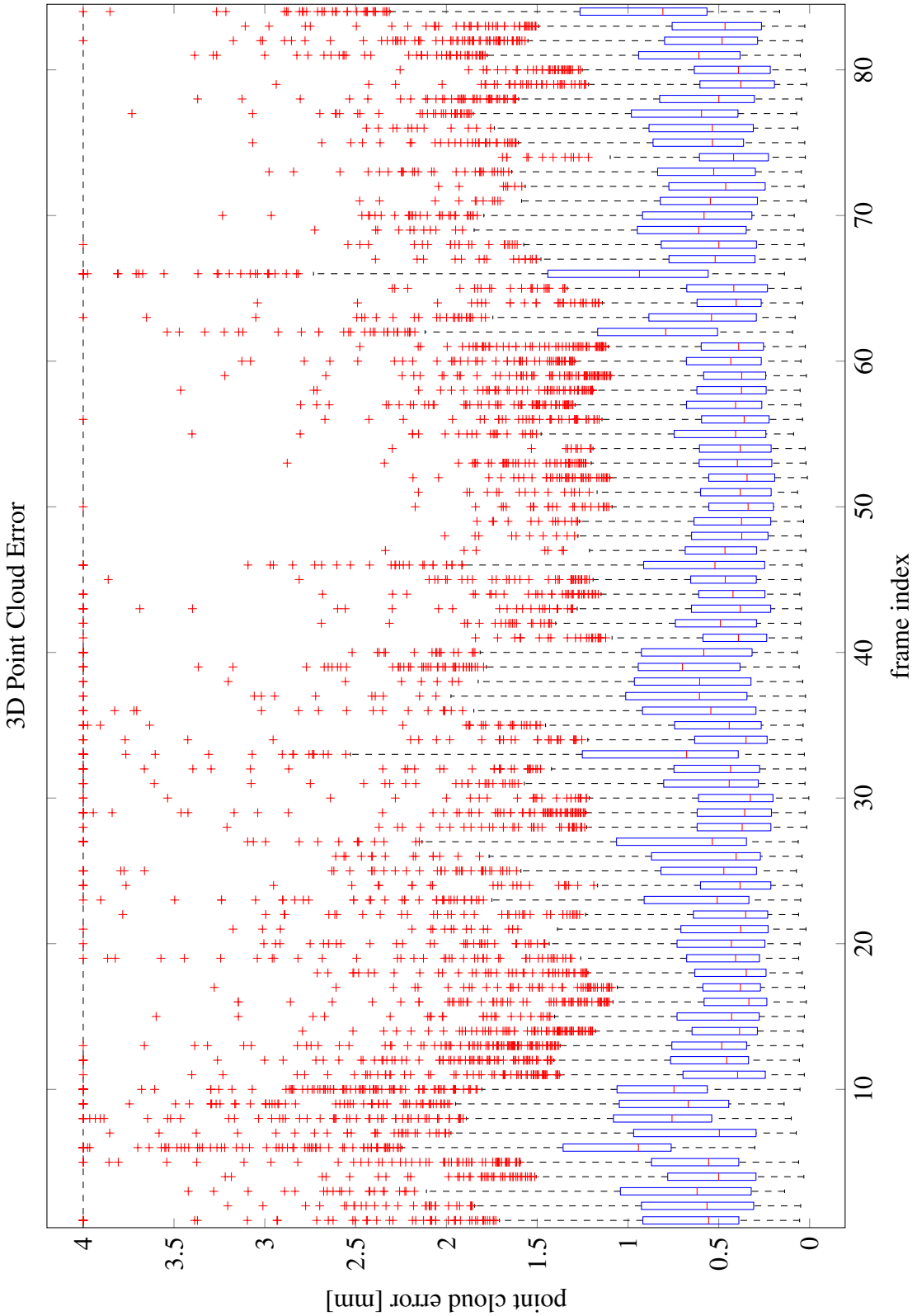

Figure C.1: Evaluation results of the sparse reconstruction of Phantom 1 Sequence 1.

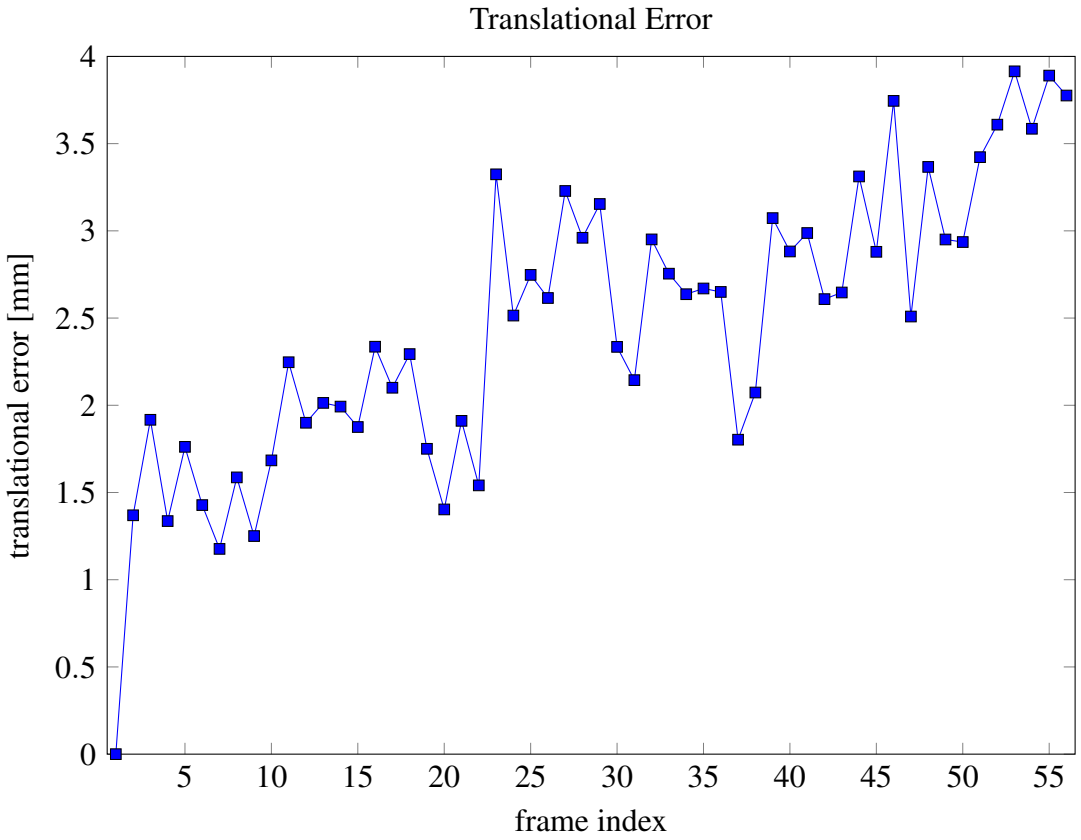
Translational Error
translational error [mm]
frame index
0
0.5
1
1.5
2
2.5
3
3.5
4
5
10
15
20
25
30
35
40
45
50
55

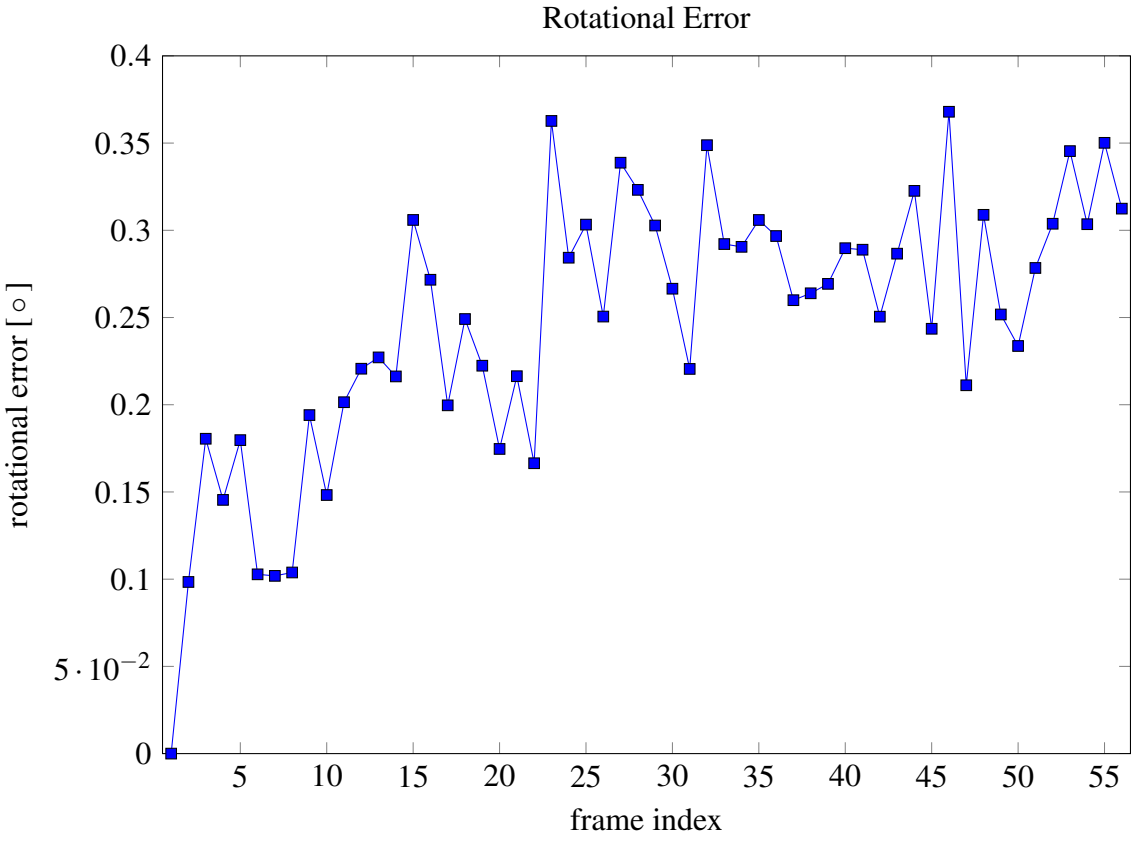
Rotational Error
rotational error [◦]
frame index
0
5 · 10−2
0.1
0.15
0.2
0.25
0.3
0.35
0.4
5
10
15
20
25
30
35
40
45
50
55

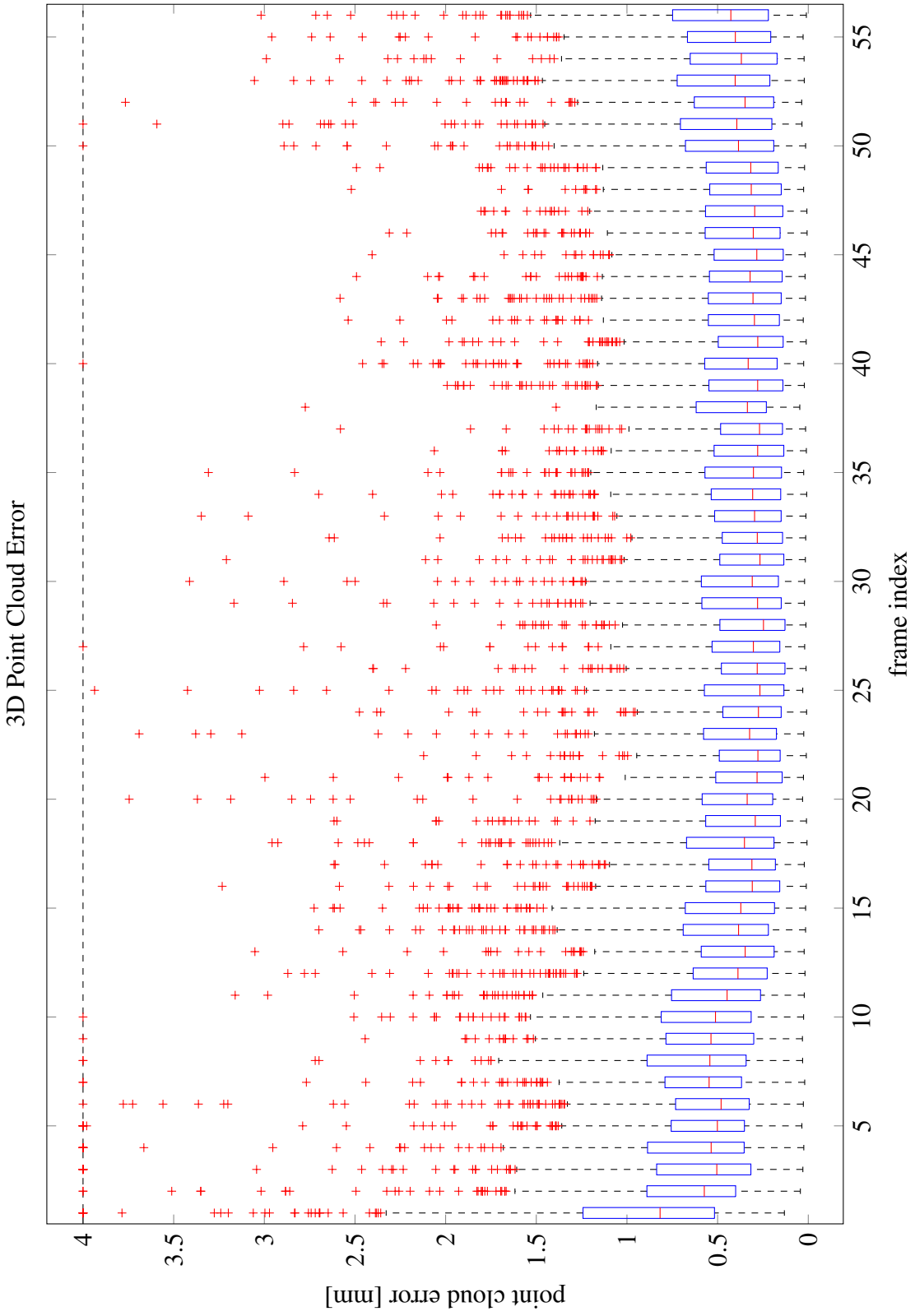

Figure C.2: Evaluation results of the sparse reconstruction of Phantom 1 Sequence 2.

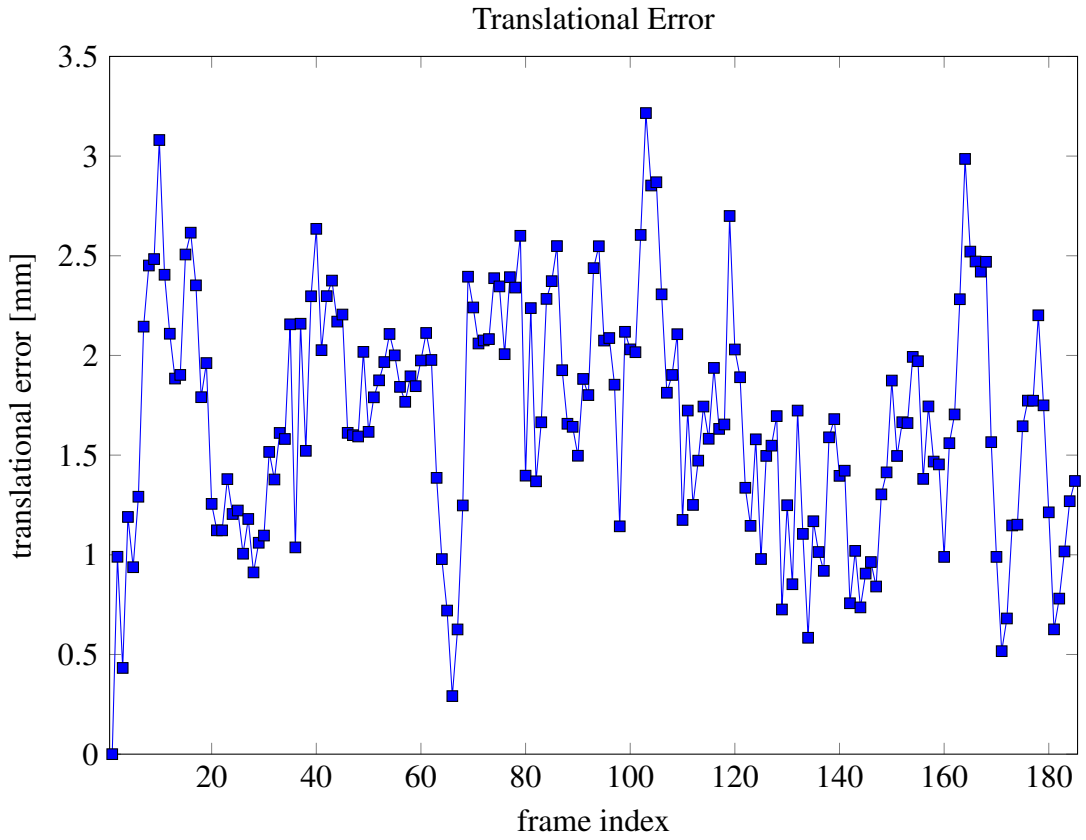
Translational Error
translational error [mm]
frame index
0
0.5
1
1.5
2
2.5
3
3.5
20
40
60
80
100
120
140
160
180

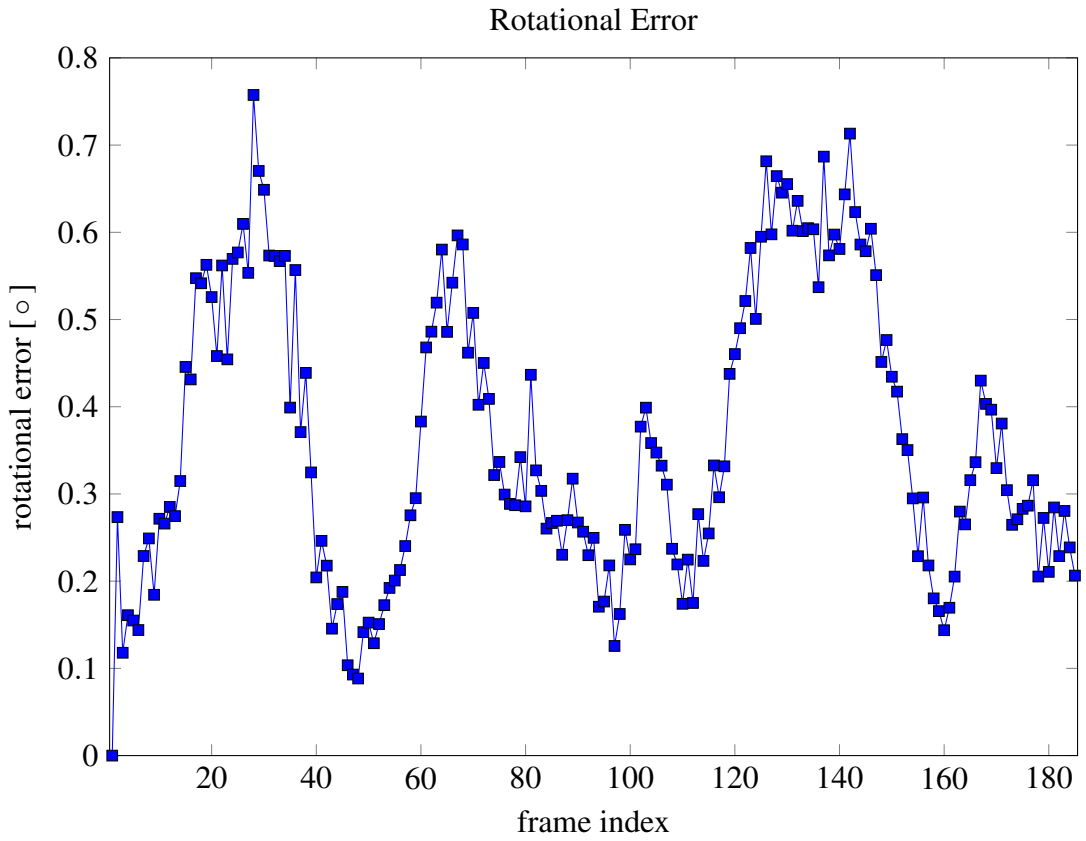
Rotational Error
rotational error [○]
frame index
0
0.1
0.2
0.3
0.4
0.5
0.6
0.7
0.8
20
40
60
80
100
120
140
160
180

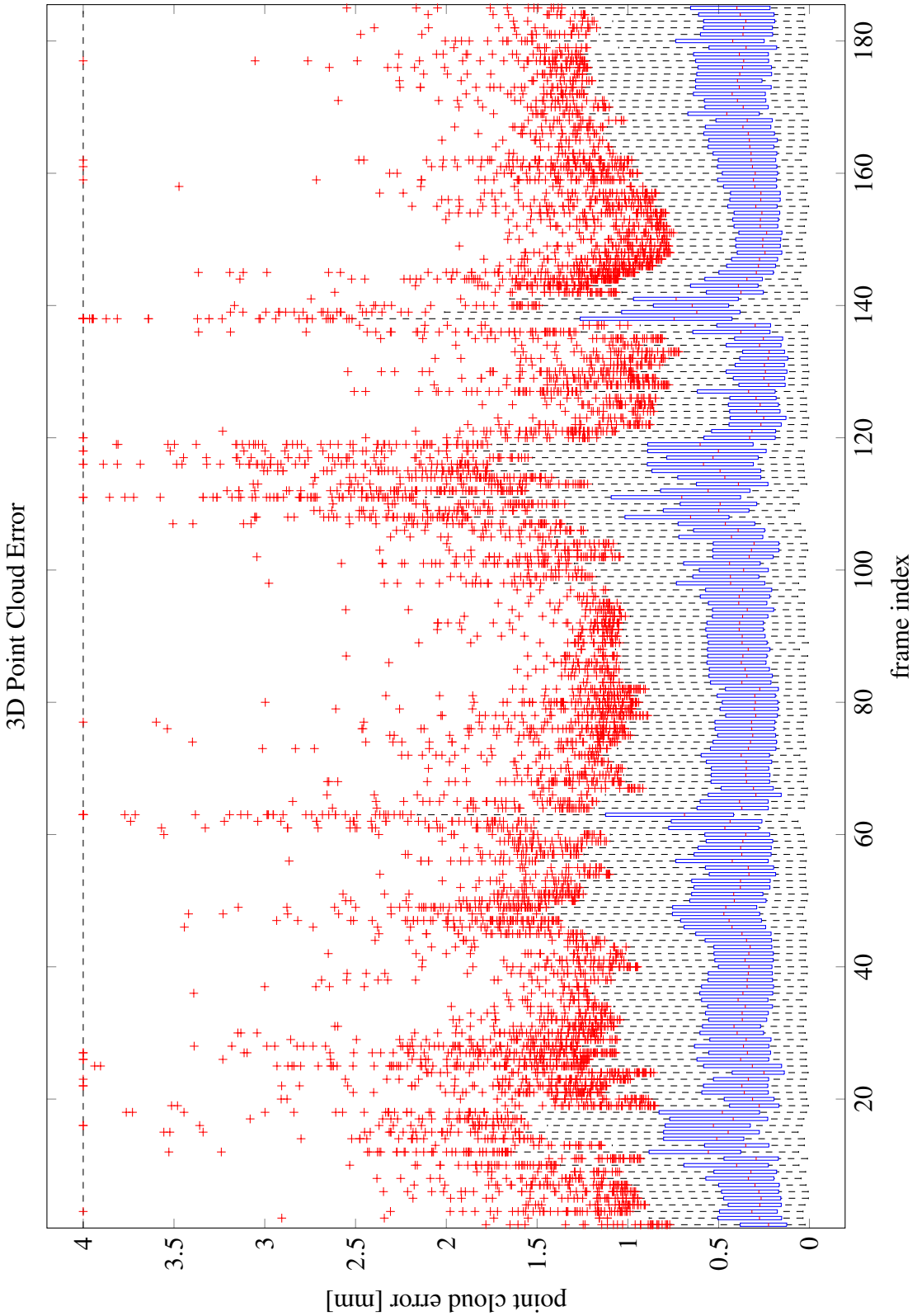

Figure C.3: Evaluation results of the sparse reconstruction of Phantom 1 Sequence 3.

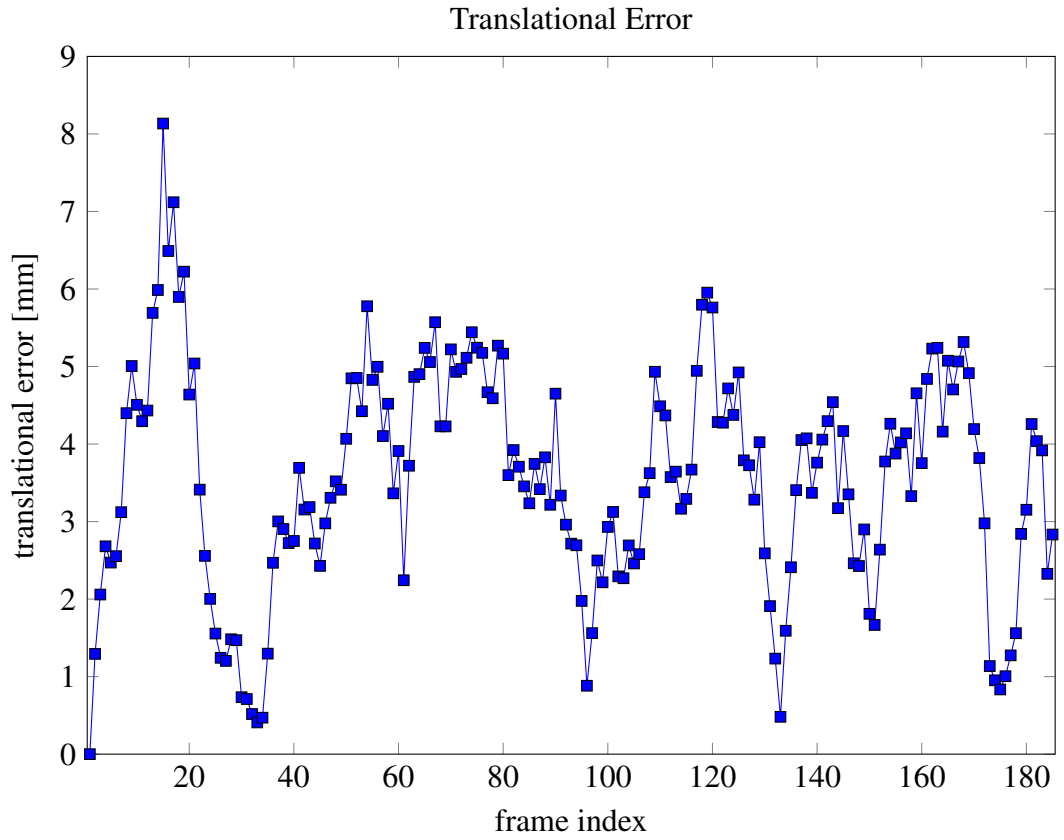
Translational Error
translational error [mm]
frame index
0
1
2
3
4
5
6
7
8
9
20
40
60
80
100
120
140
160
180

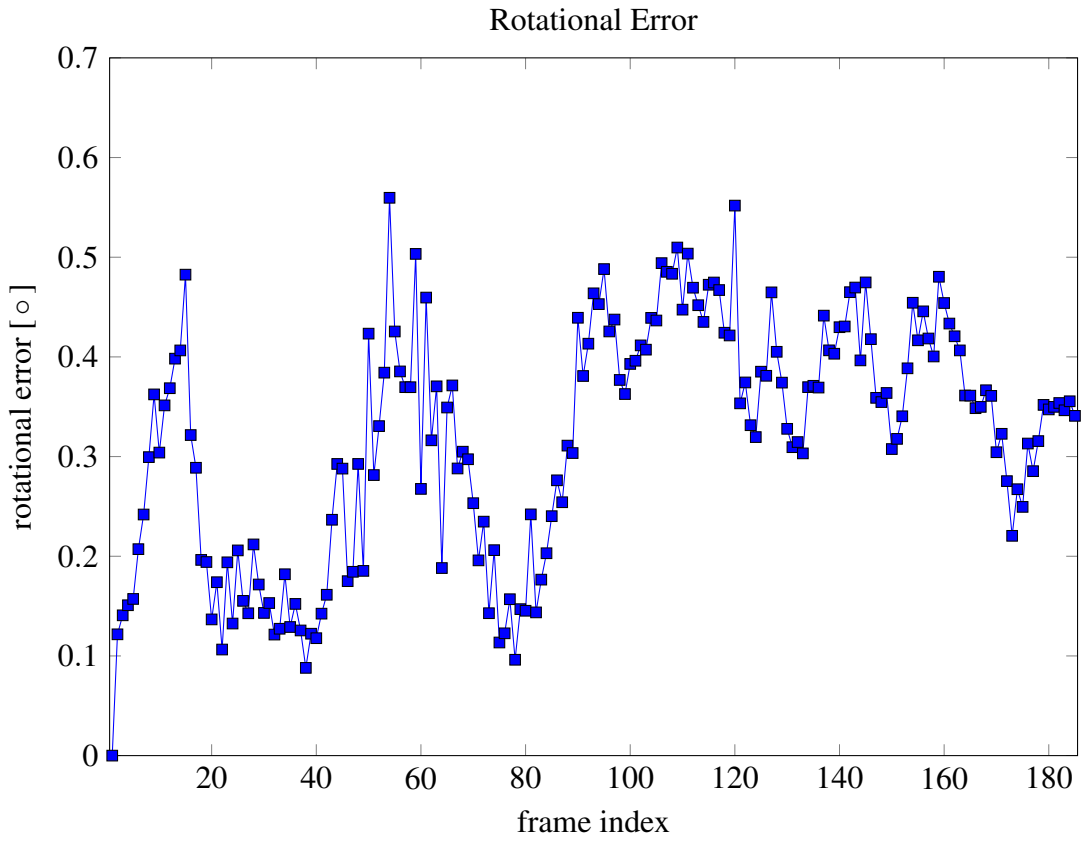
Rotational Error
rotational error [○]
frame index
0
0.1
0.2
0.3
0.4
0.5
0.6
0.7
20
40
60
80
100
120
140
160
180

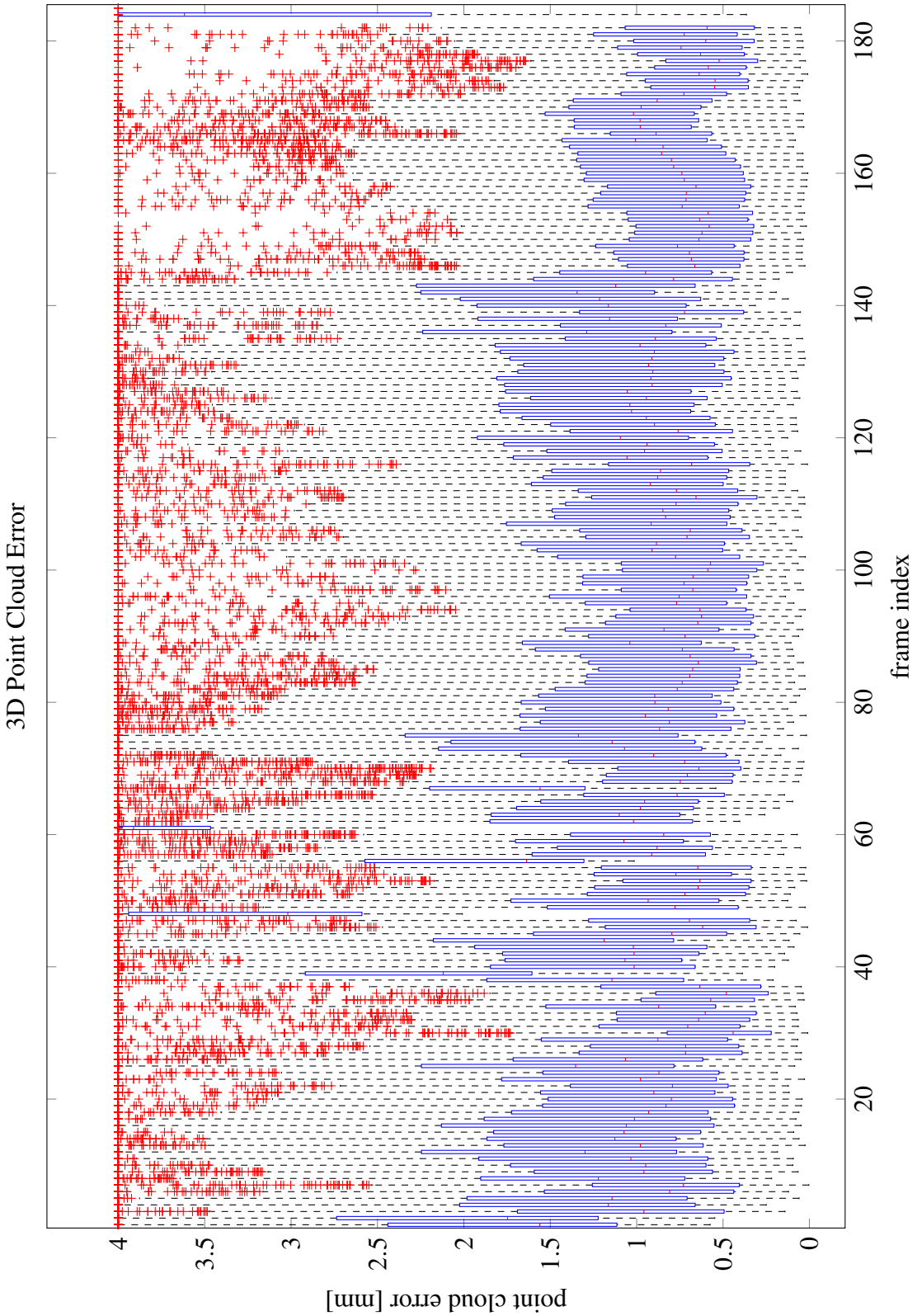

Figure C.4: Evaluation results of the sparse reconstruction of Phantom 1 Sequence 4.

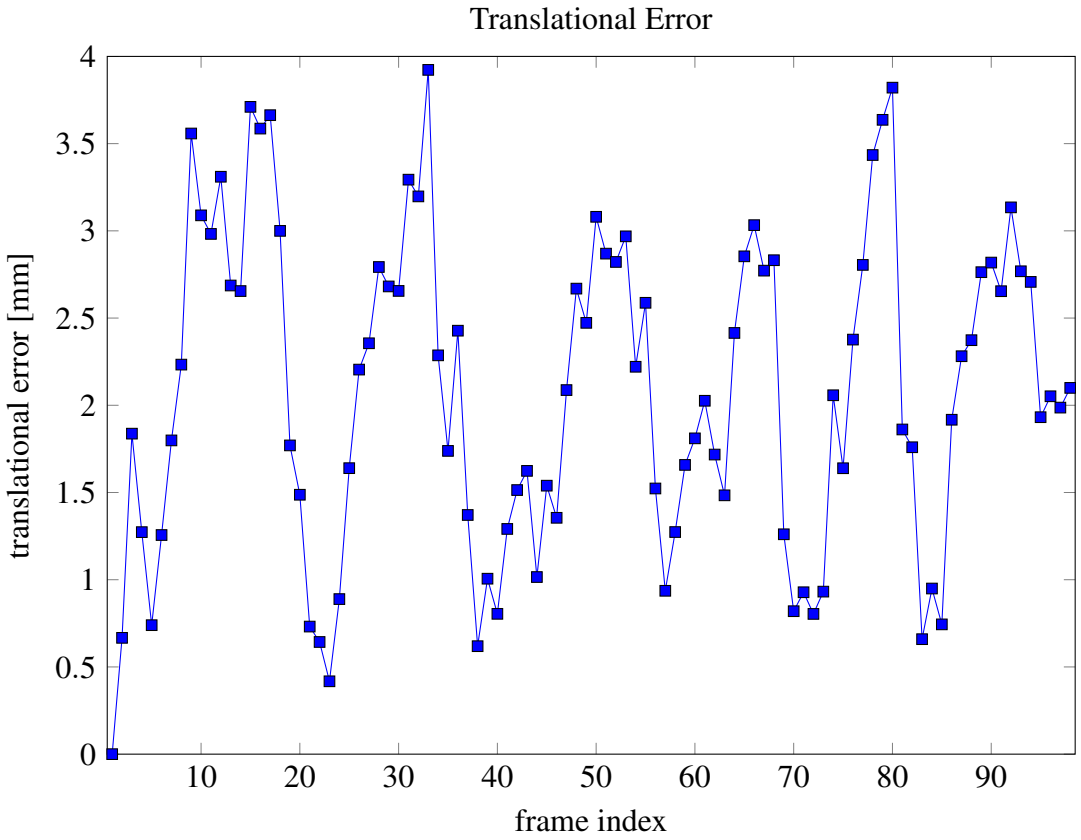
Translational Error
translational error [mm]
frame index
0
0.5
1
1.5
2
2.5
3
3.5
4
10
20
30
40
50
60
70
80
90

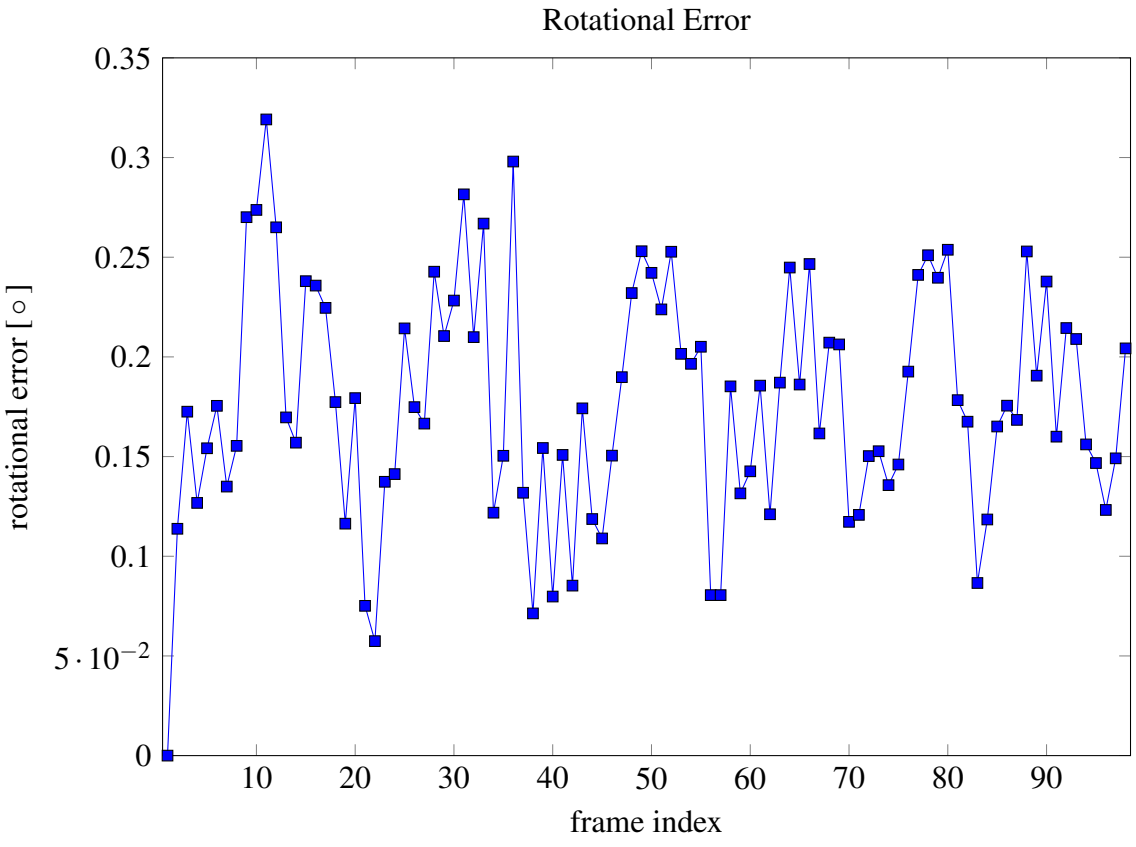
Rotational Error
rotational error [◦]
frame index
0
5 · 10−2
0.1
0.15
0.2
0.25
0.3
0.35
10
20
30
40
50
60
70
80
90

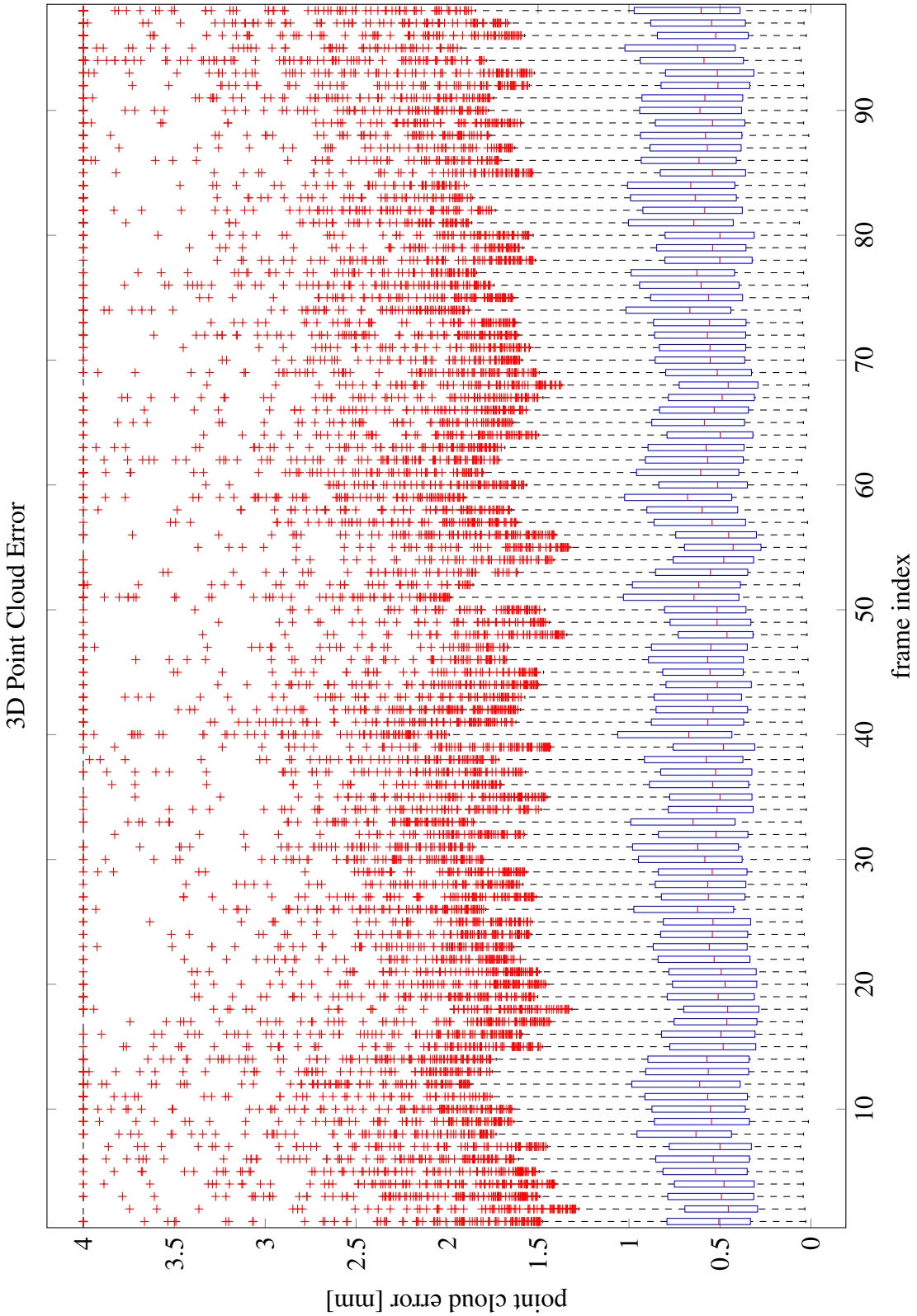

Figure C.5: Evaluation results of the sparse reconstruction of Phantom 1 Sequence 5.

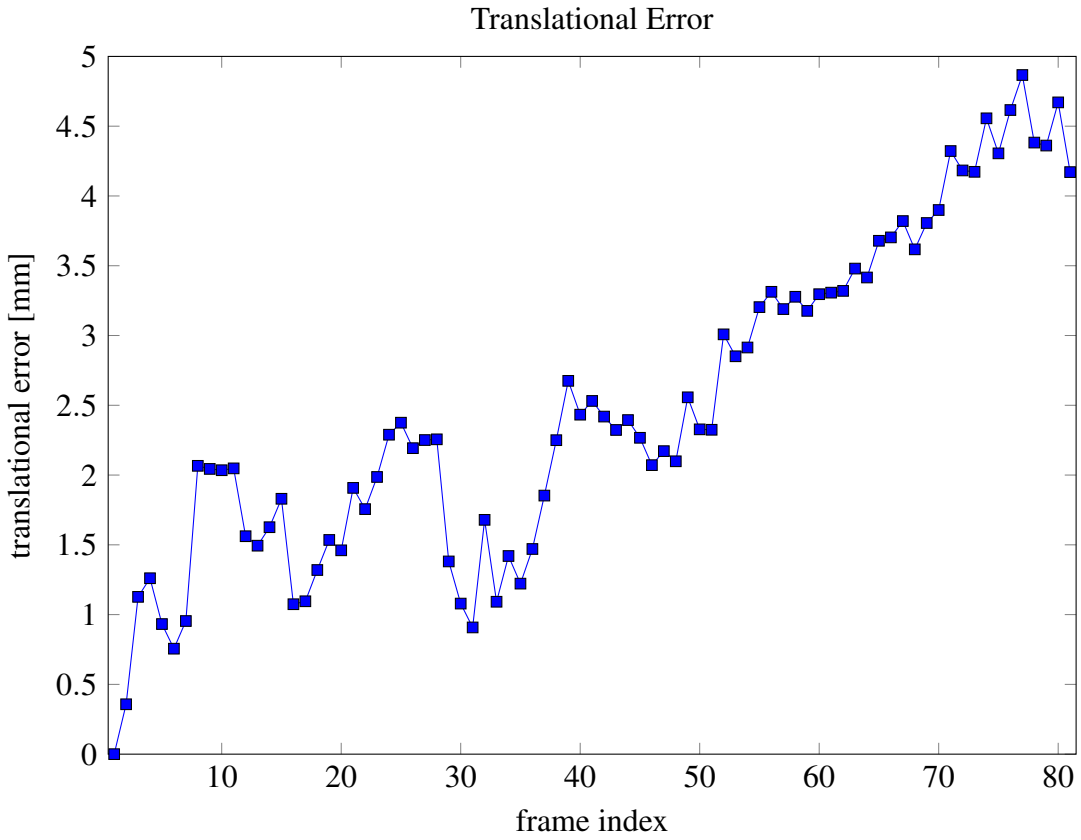
Translational Error
translational error [mm]
frame index
0
0.5
1
1.5
2
2.5
3
3.5
4
4.5
5
10
20
30
40
50
60
70
80

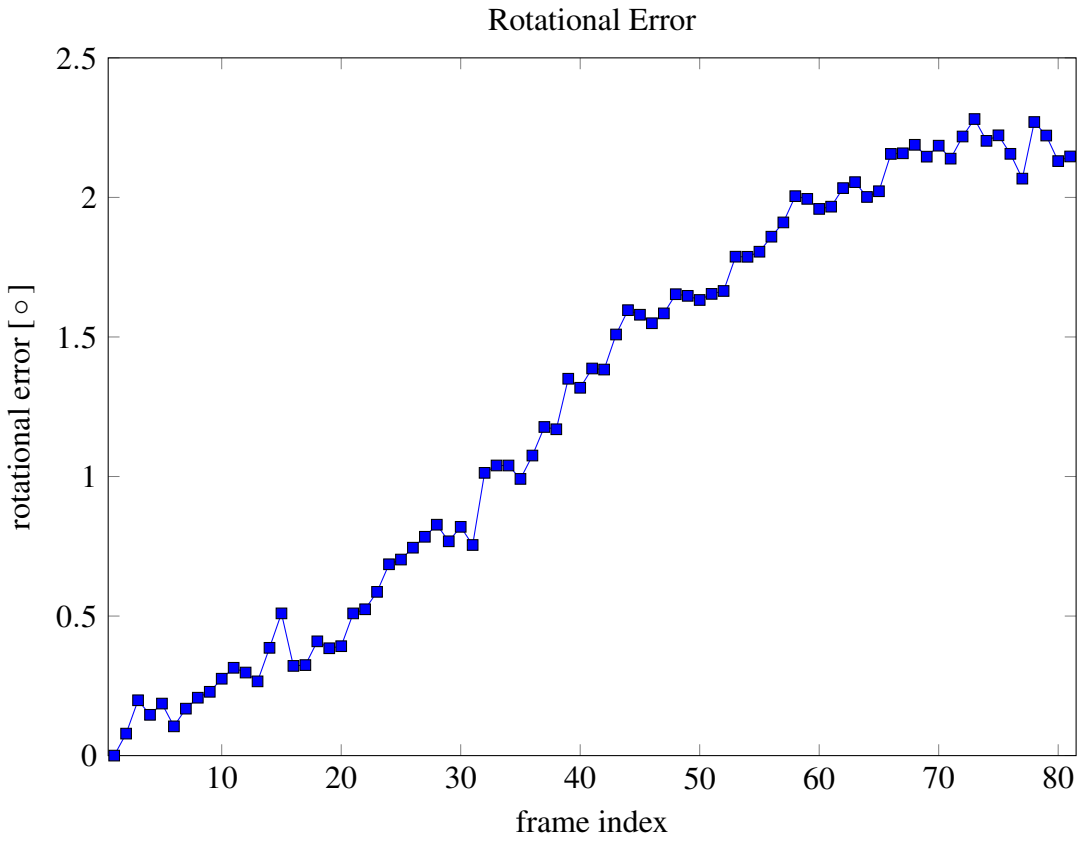
Rotational Error
rotational error [○]
frame index
0
0.5
1
1.5
2
2.5
10
20
30
40
50
60
70
80

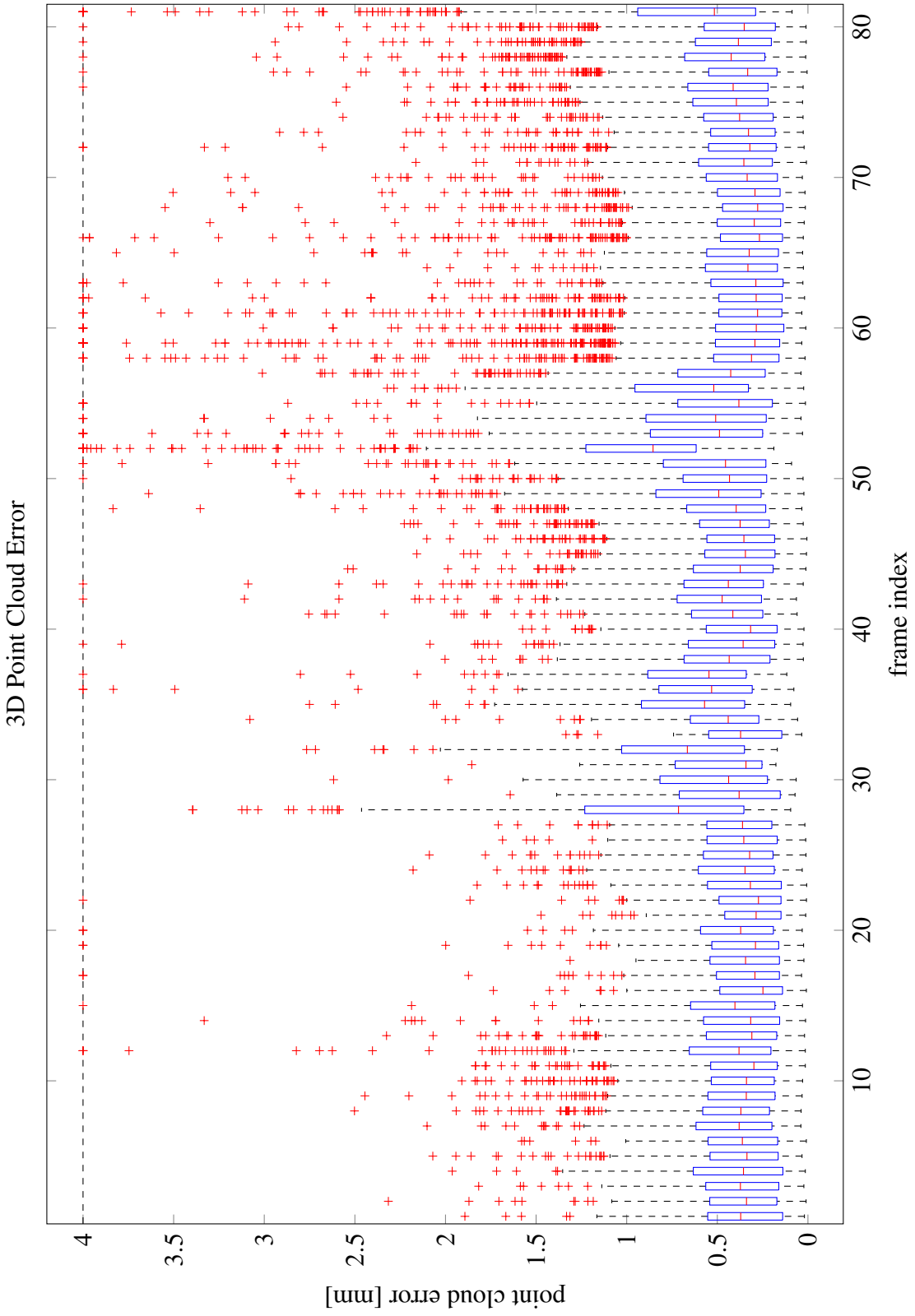

Figure C.6: Evaluation results of the sparse reconstruction of Phantom 2 Sequence 1.

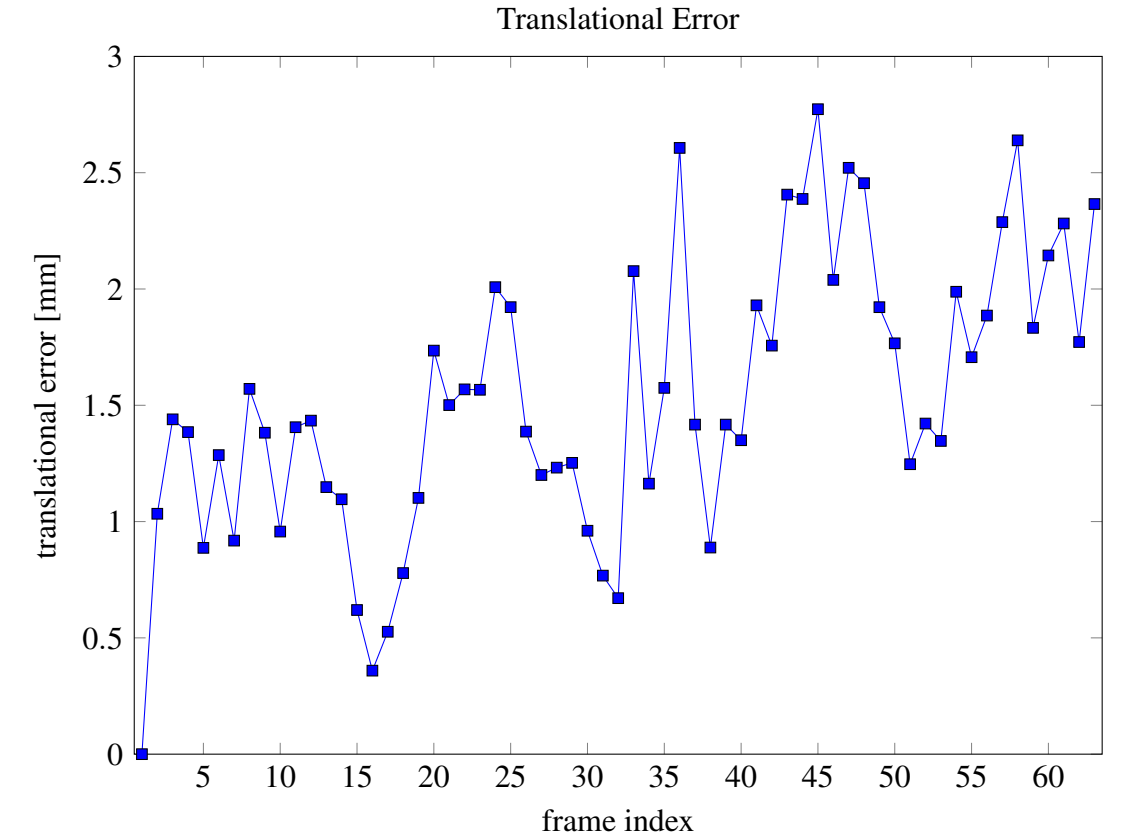
Translational Error
translational error [mm]
frame index
0
0.5
1
1.5
2
2.5
3
5
10
15
20
25
30
35
40
45
50
55
60

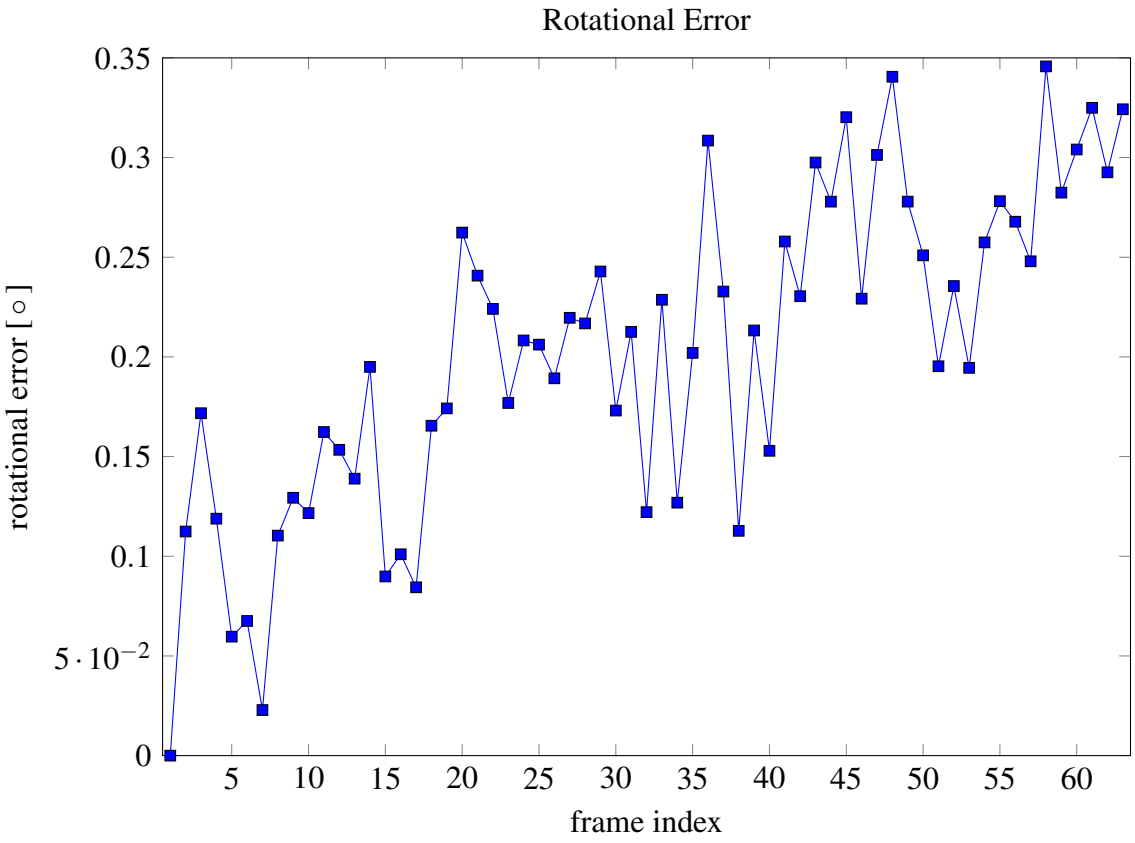
Rotational Error
rotational error [◦]
frame index
0
5 · 10−2
0.1
0.15
0.2
0.25
0.3
0.35
5
10
15
20
25
30
35
40
45
50
55
60

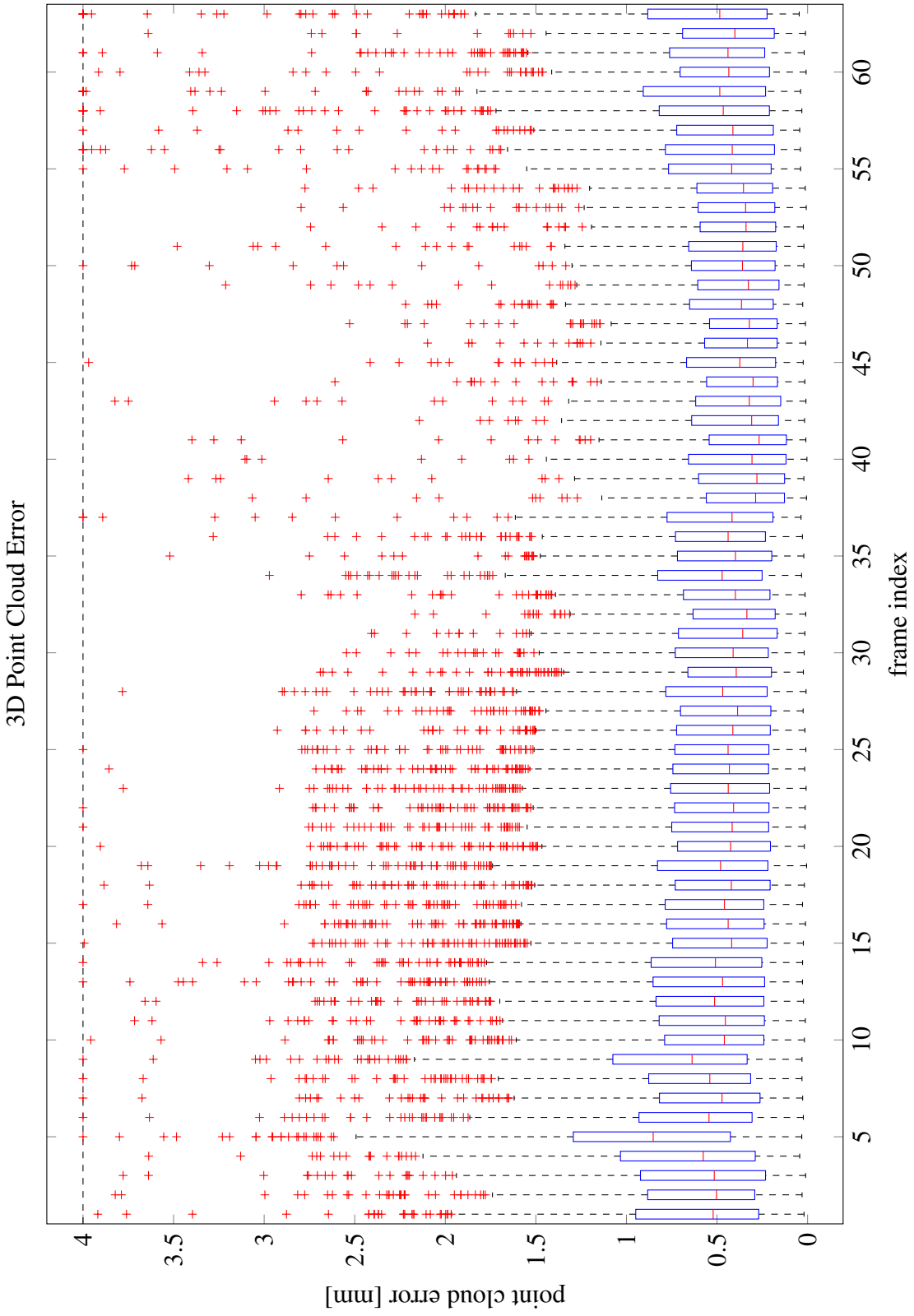

Figure C.7: Evaluation results of the sparse reconstruction of Phantom 2 Sequence 2.

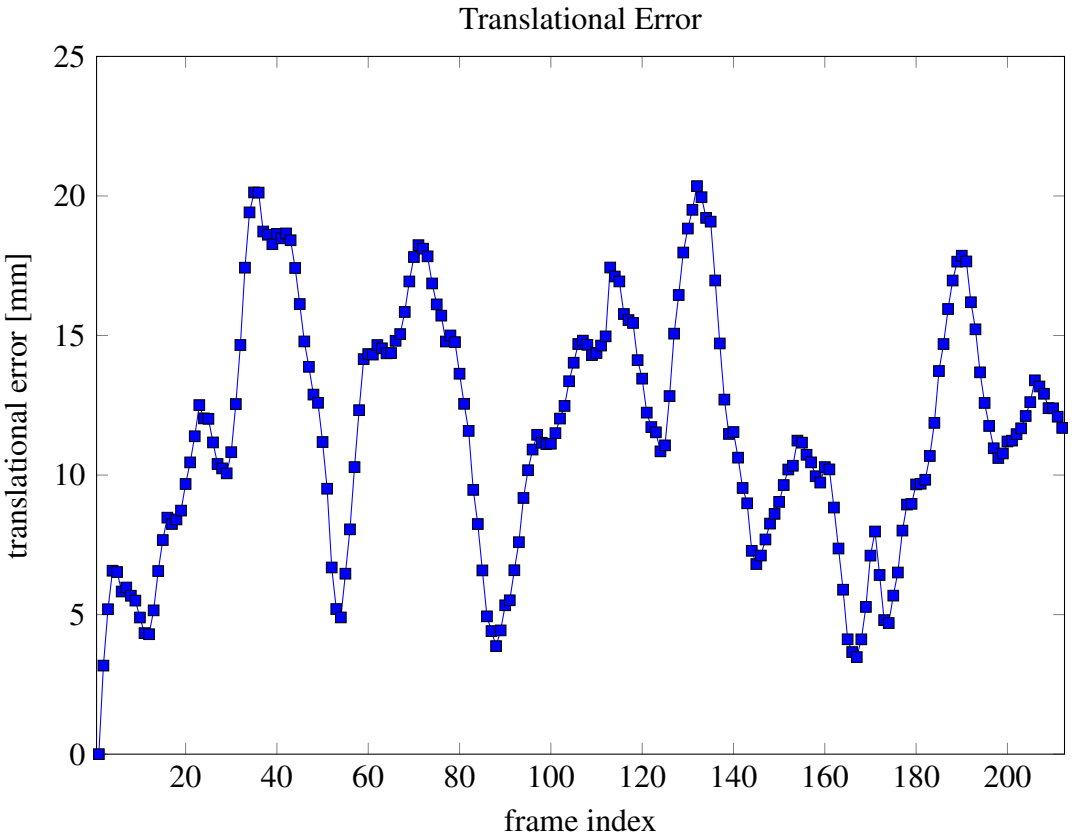
Translational Error
translational error [mm]
frame index
0
5
10
15
20
25
20
40
60
80
100
120
140
160
180
200

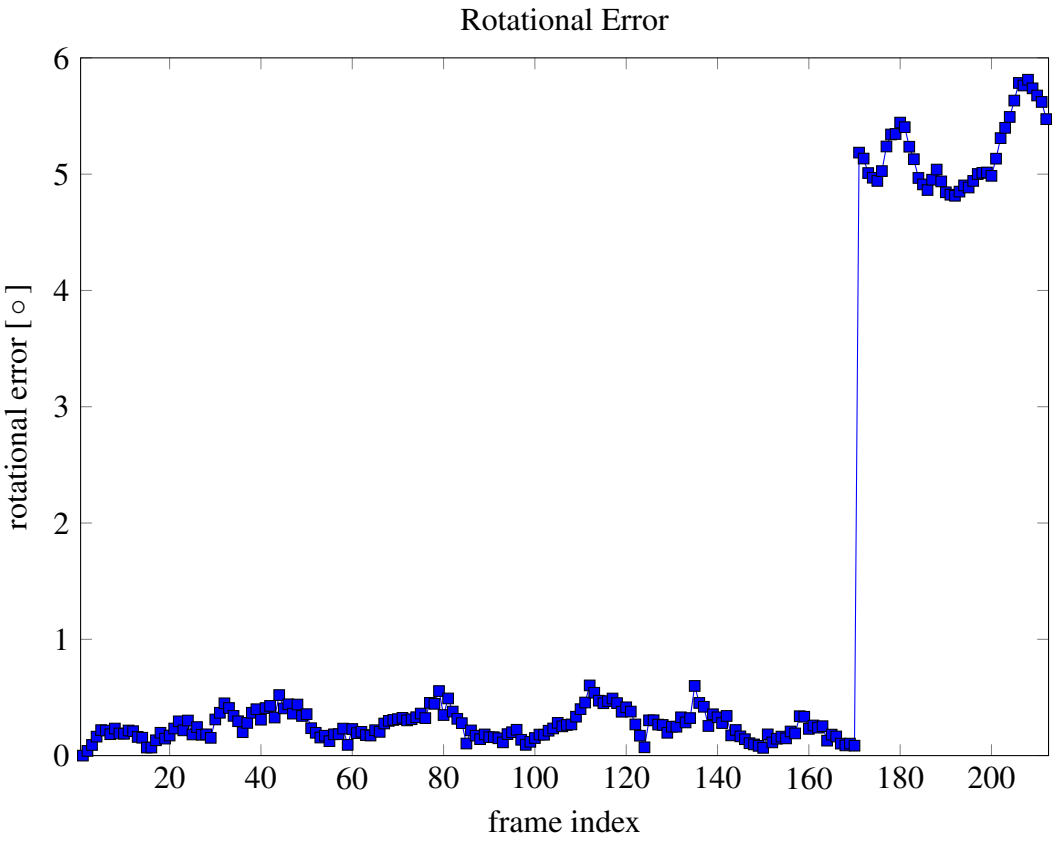
Rotational Error
rotational error [◦]
frame index
0
1
2
3
4
5
6
20
40
60
80
100
120
140
160
180
200

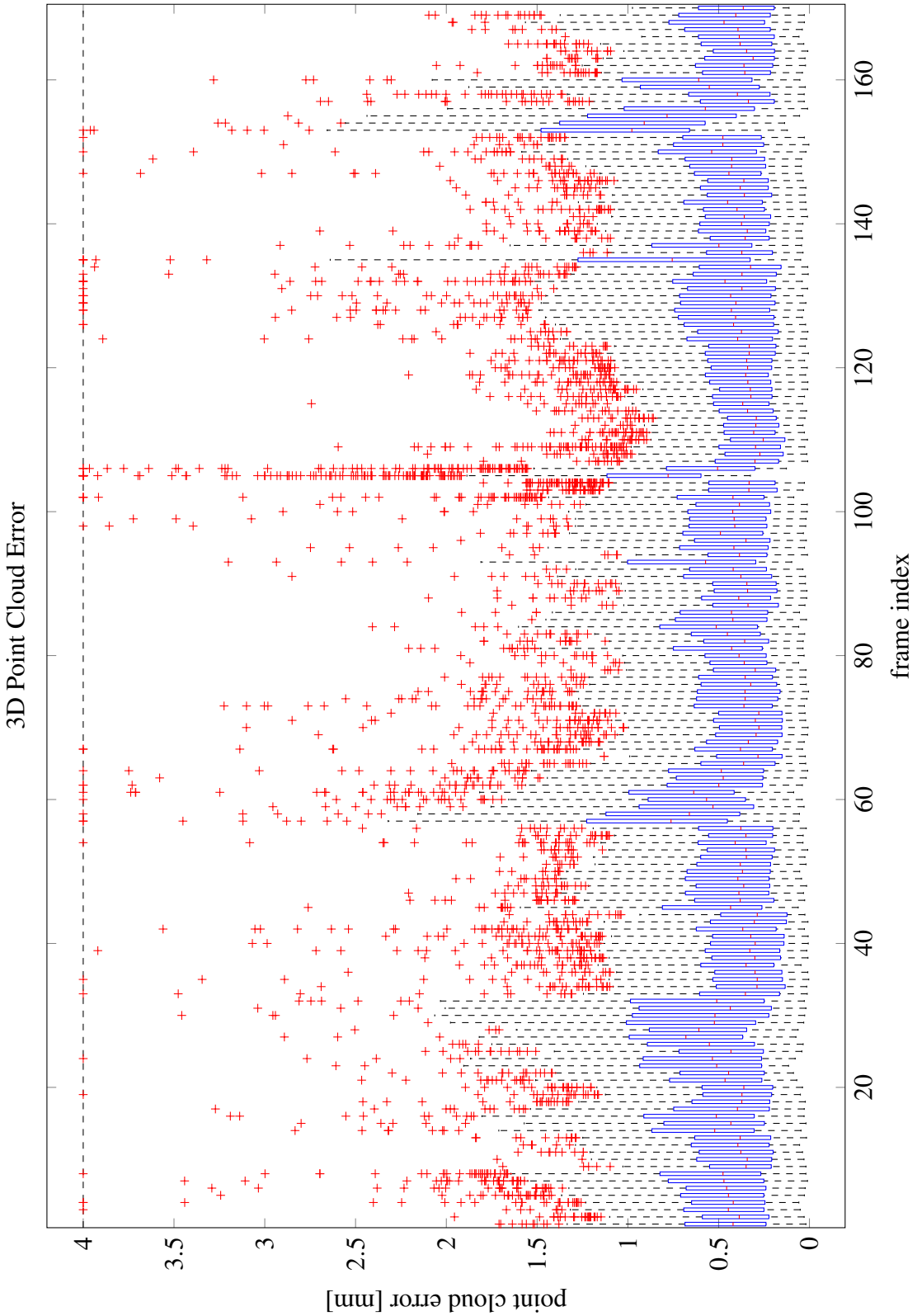

Figure C.8: Evaluation results of the sparse reconstruction of Phantom 2 Sequence 3.

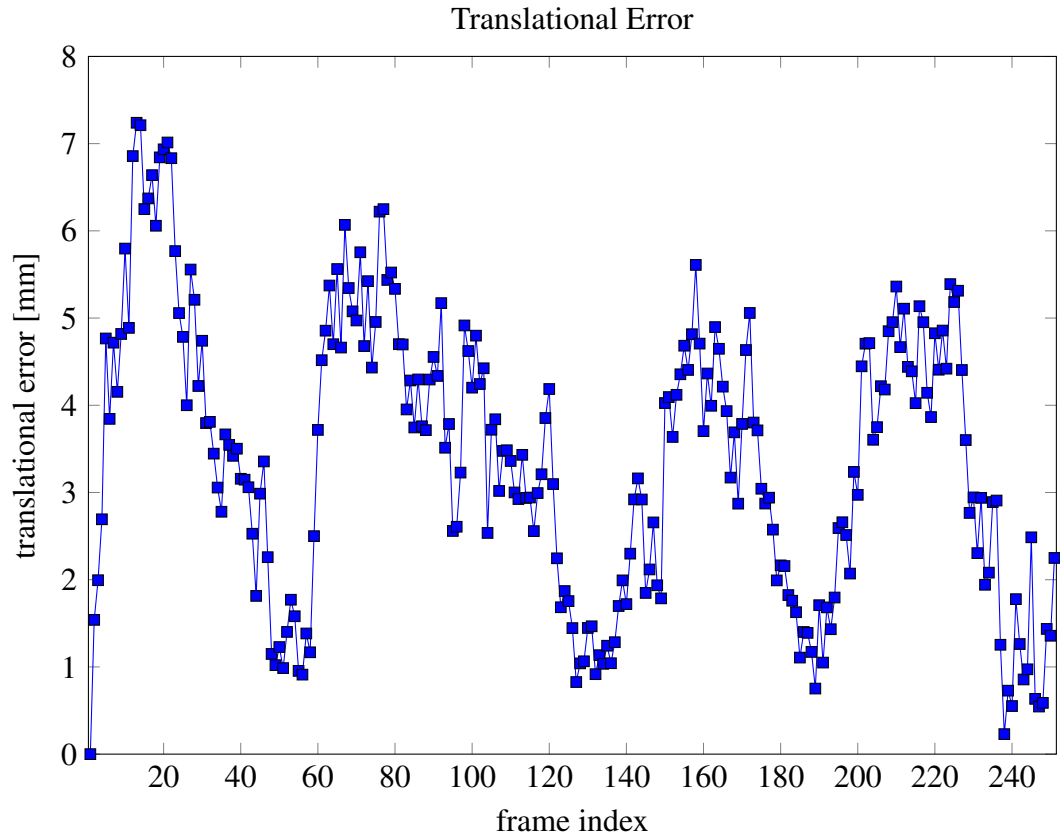
Translational Error
translational error [mm]
frame index
0
1
2
3
4
5
6
7
8
20
40
60
80
100
120
140
160
180
200
220
240

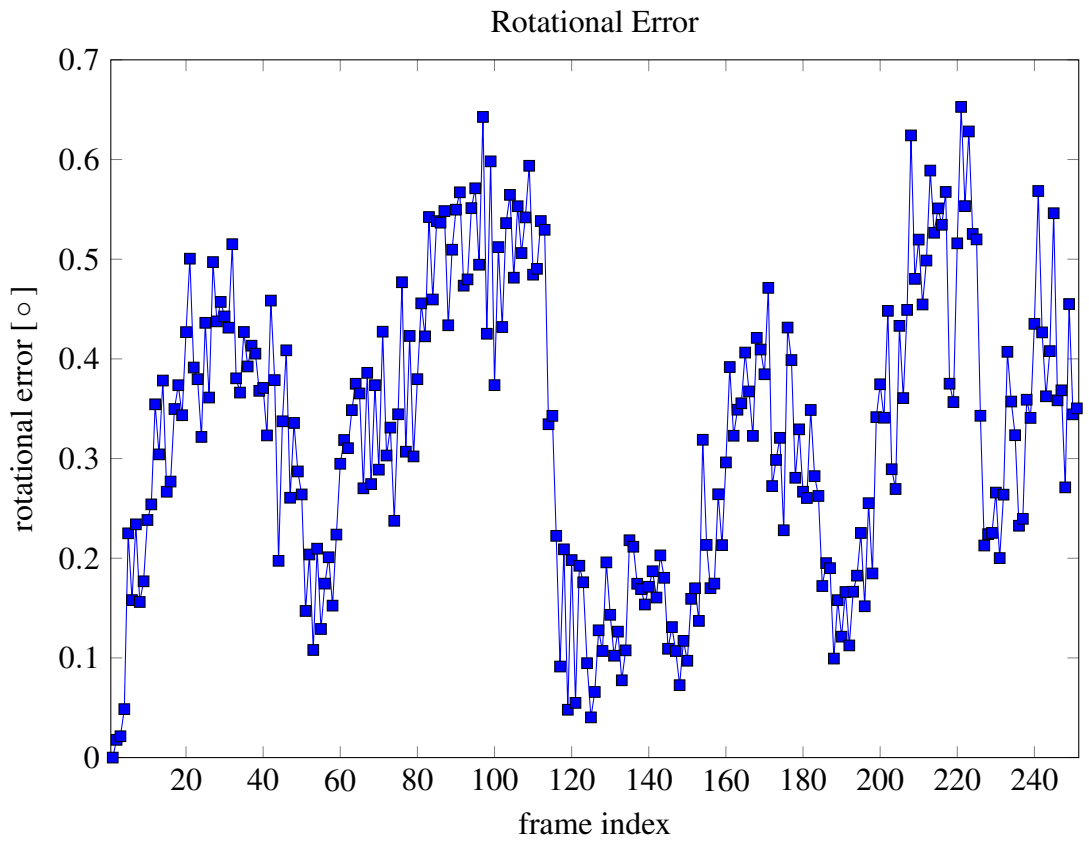
Rotational Error
rotational error [○]
frame index
0
0.1
0.2
0.3
0.4
0.5
0.6
0.7
20
40
60
80
100
120
140
160
180
200
220
240

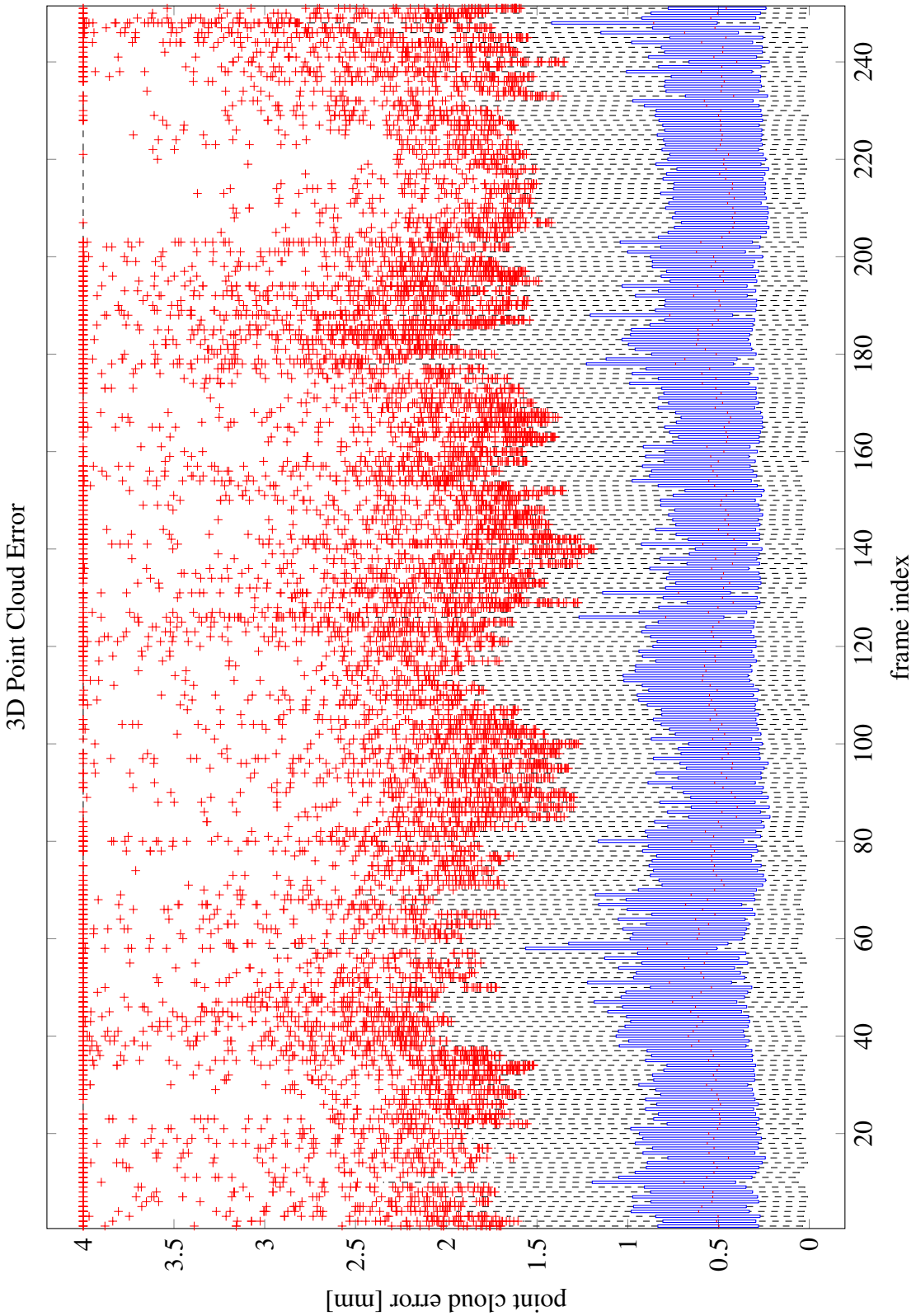

Figure C.9: Evaluation results of the sparse reconstruction of Phantom 2 Sequence 4.

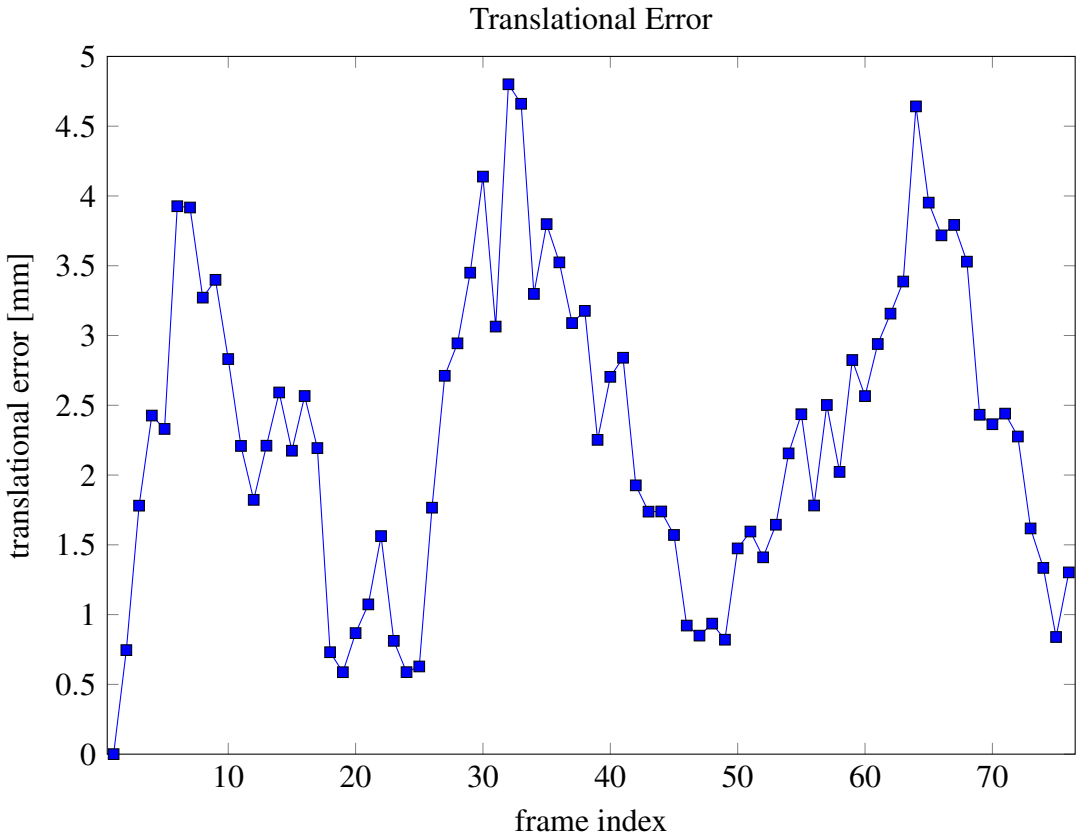
Translational Error
translational error [mm]
frame index
0
0.5
1
1.5
2
2.5
3
3.5
4
4.5
5
10
20
30
40
50
60
70

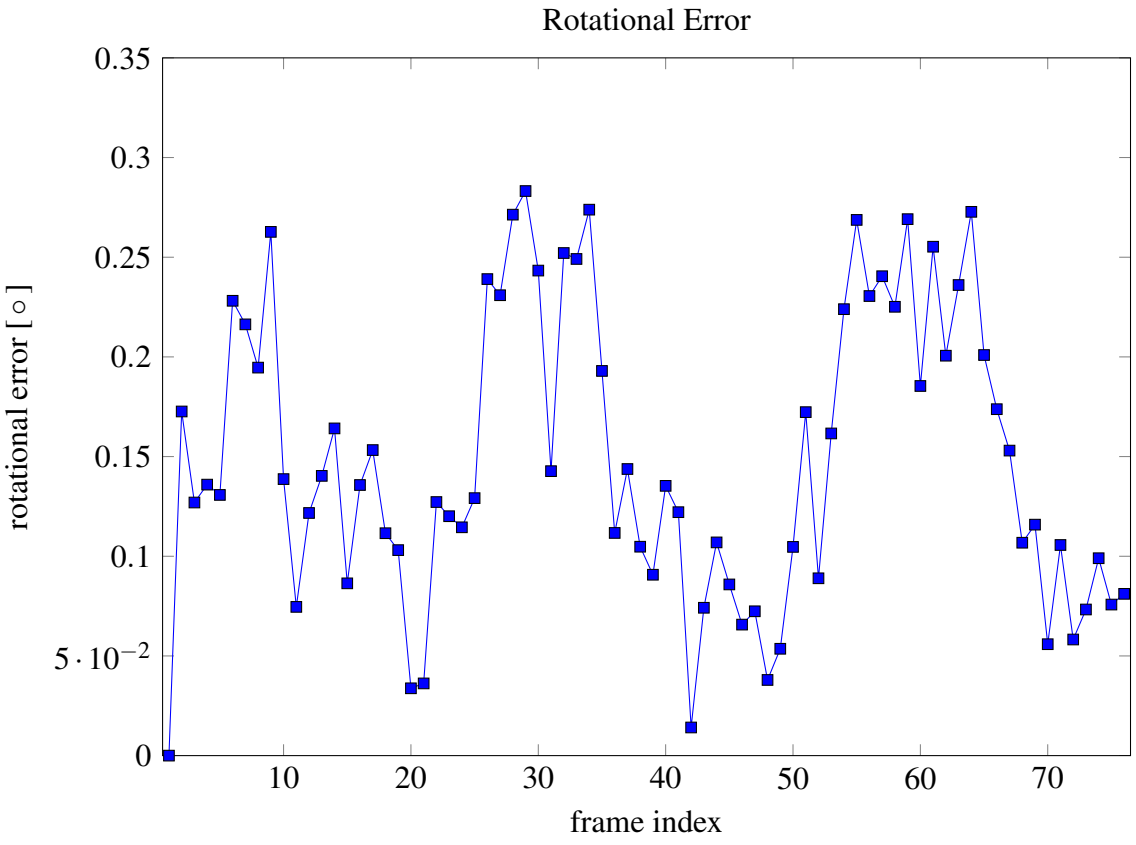
Rotational Error
rotational error [◦]
frame index
0
5 · 10−2
0.1
0.15
0.2
0.25
0.3
0.35
10
20
30
40
50
60
70

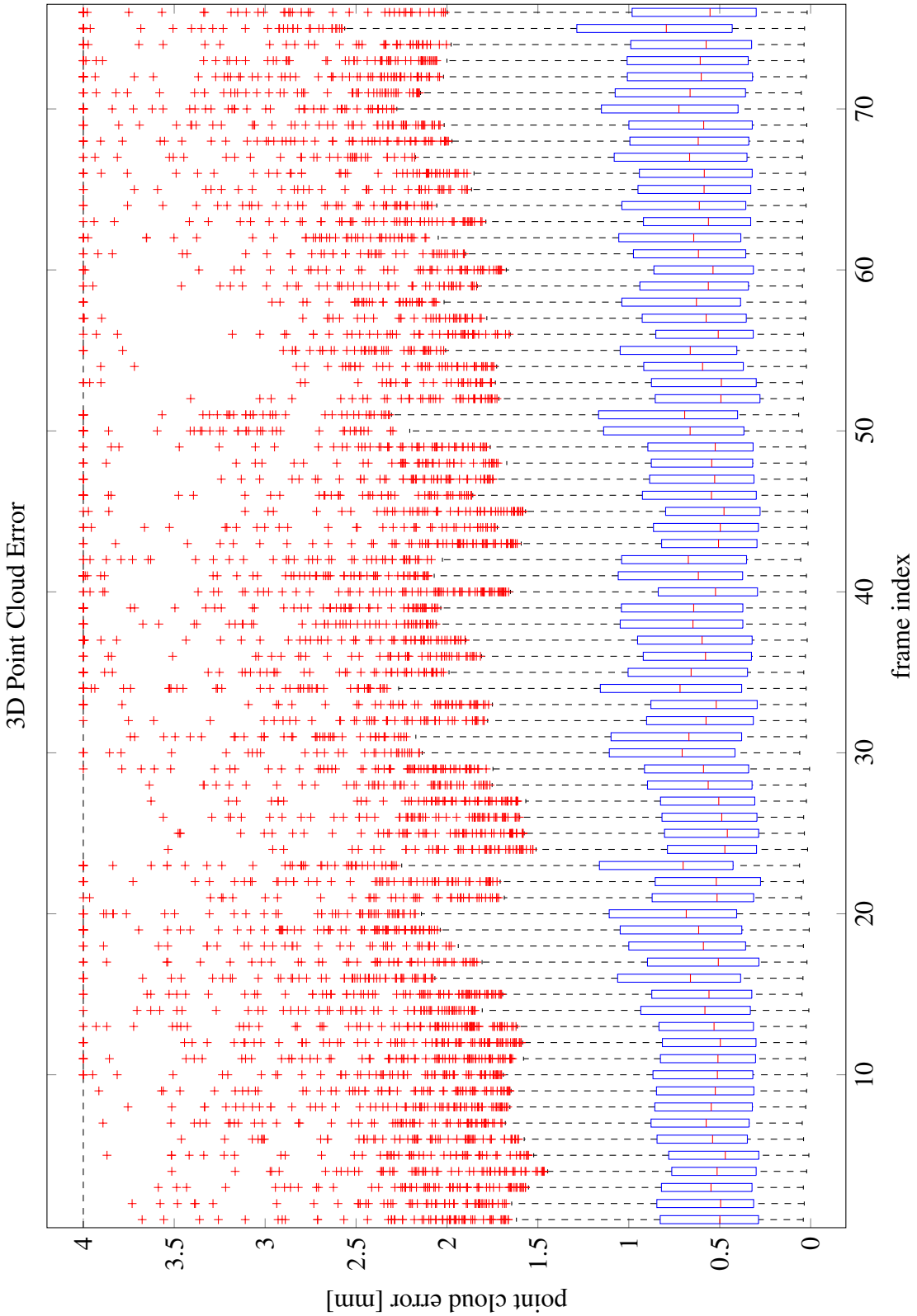

Figure C.10: Evaluation results of the sparse reconstruction of Phantom 2 Sequence 5.

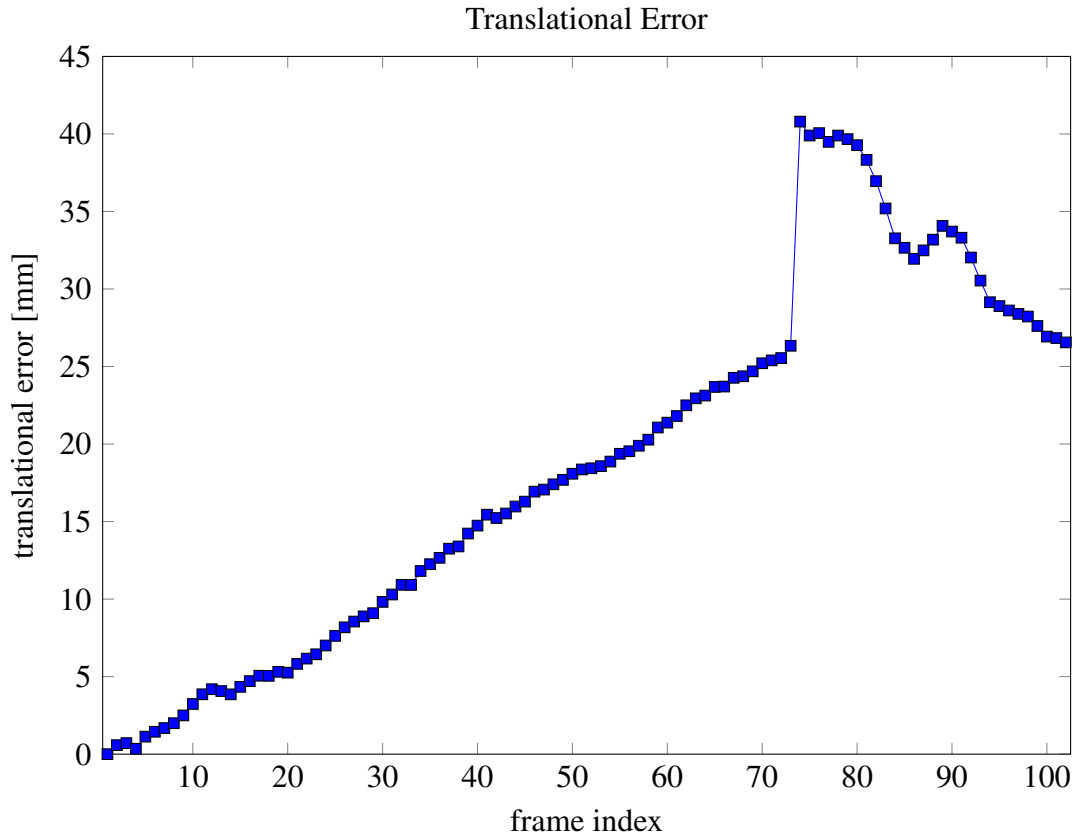
Translational Error
translational error [mm]
frame index
0
5
10
15
20
25
30
35
40
45
10
20
30
40
50
60
70
80
90
100

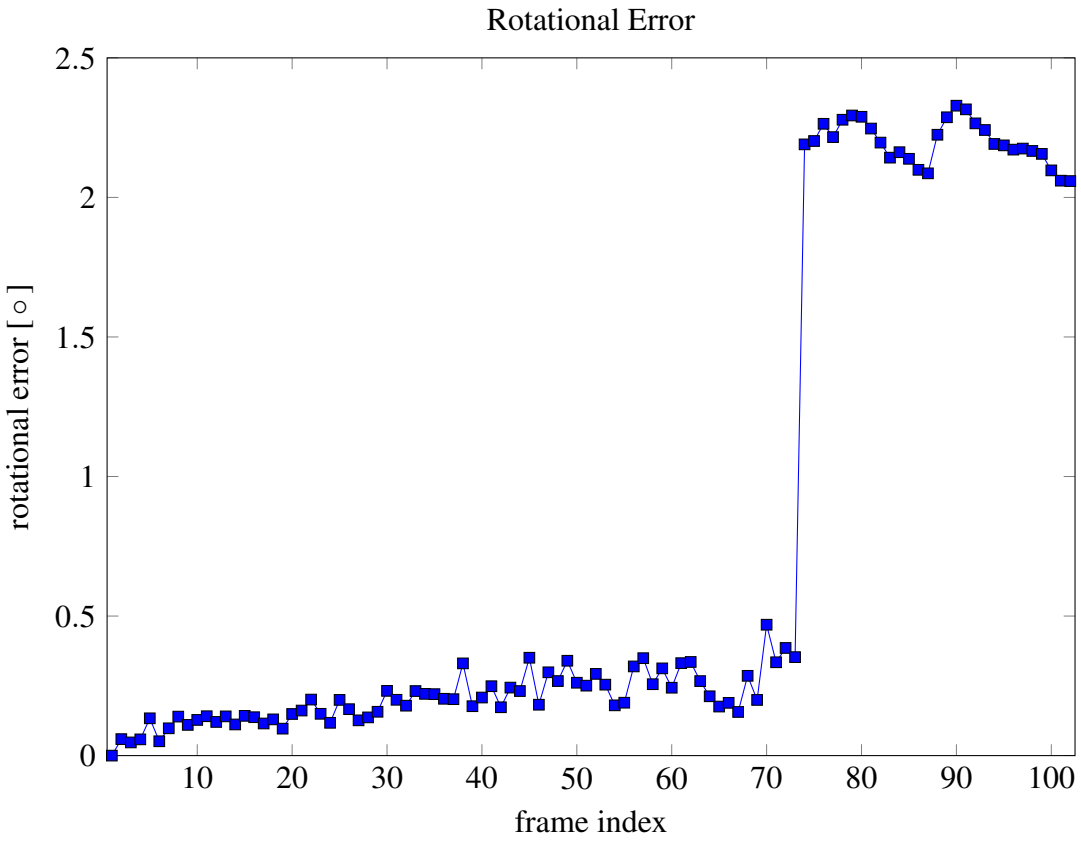
Rotational Error
rotational error [◦]
frame index
0
0.5
1
1.5
2
2.5
10
20
30
40
50
60
70
80
90
100

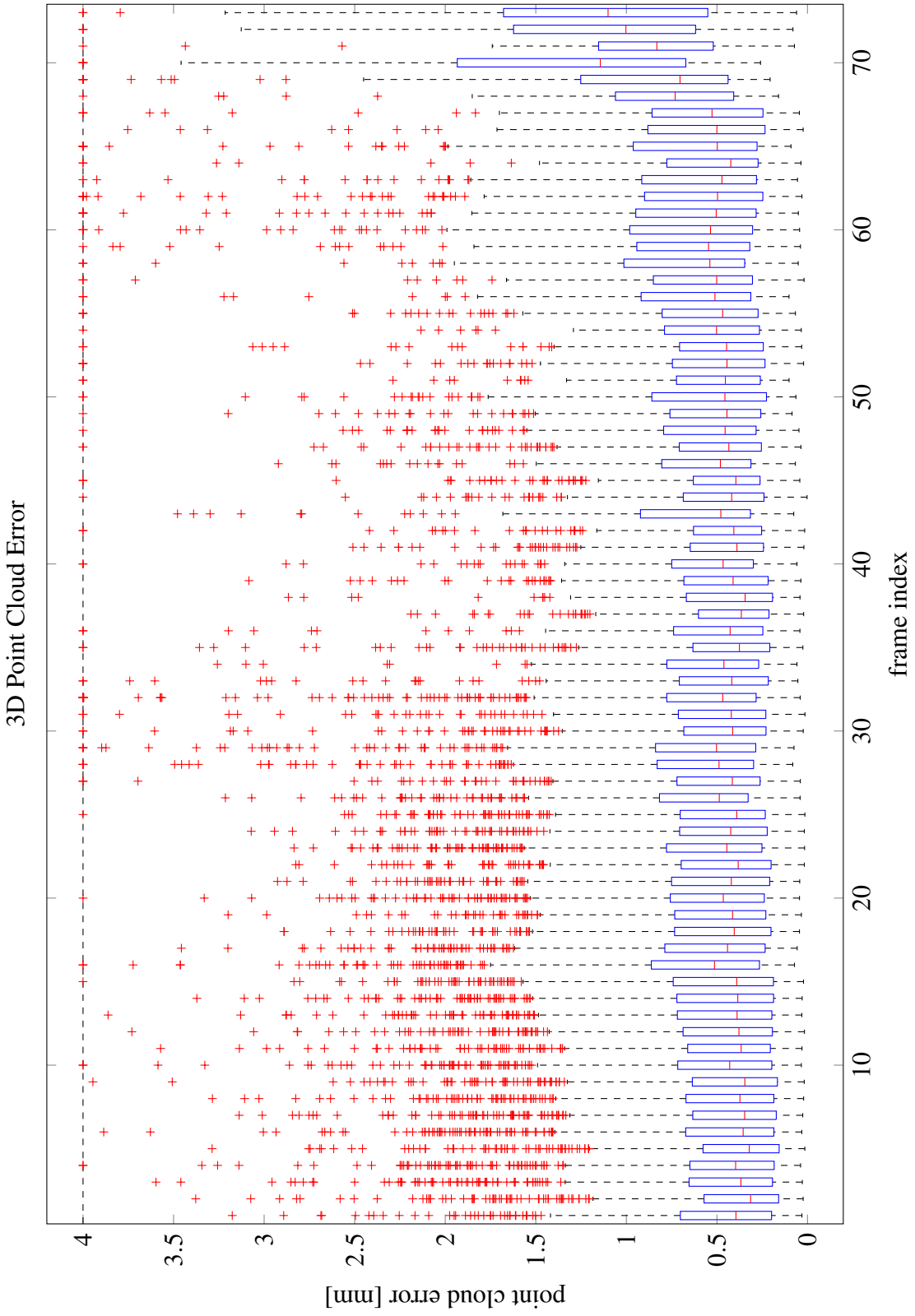

Figure C.11: Evaluation results of the sparse reconstruction of Phantom 3 Sequence 2.

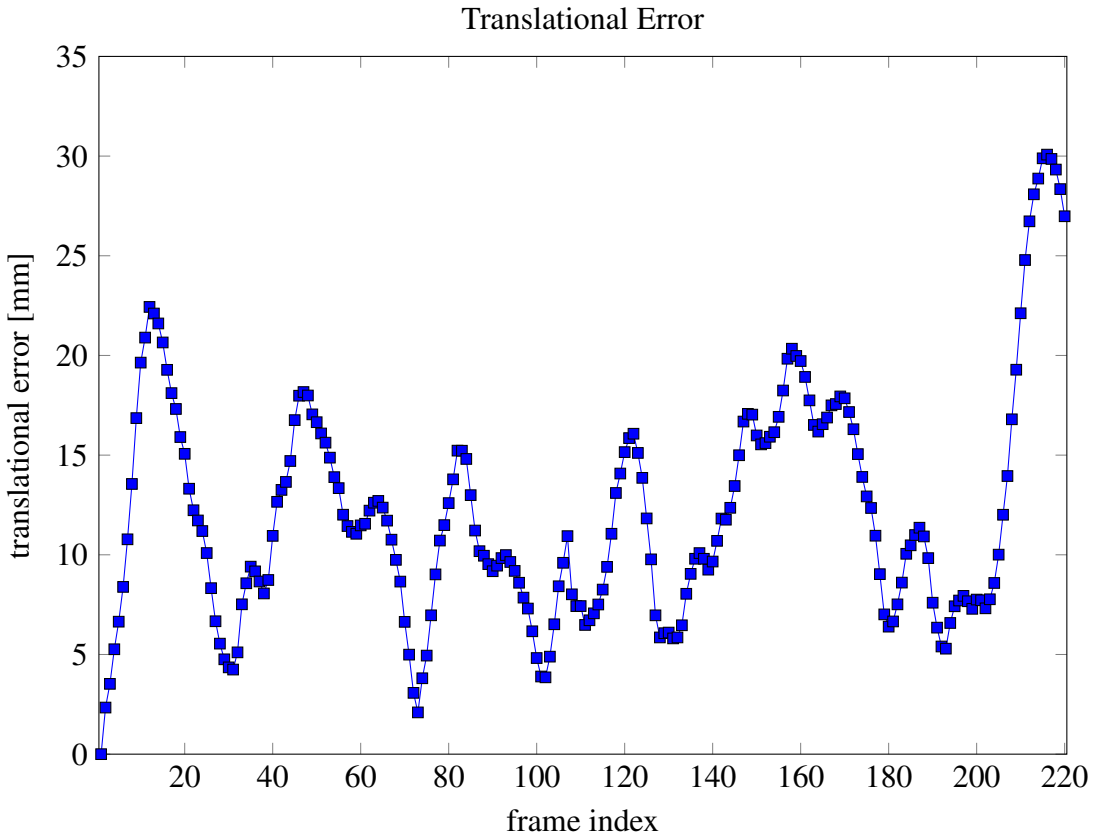
Translational Error
translational error [mm]
frame index
0
5
10
15
20
25
30
35
20
40
60
80
100
120
140
160
180
200
220

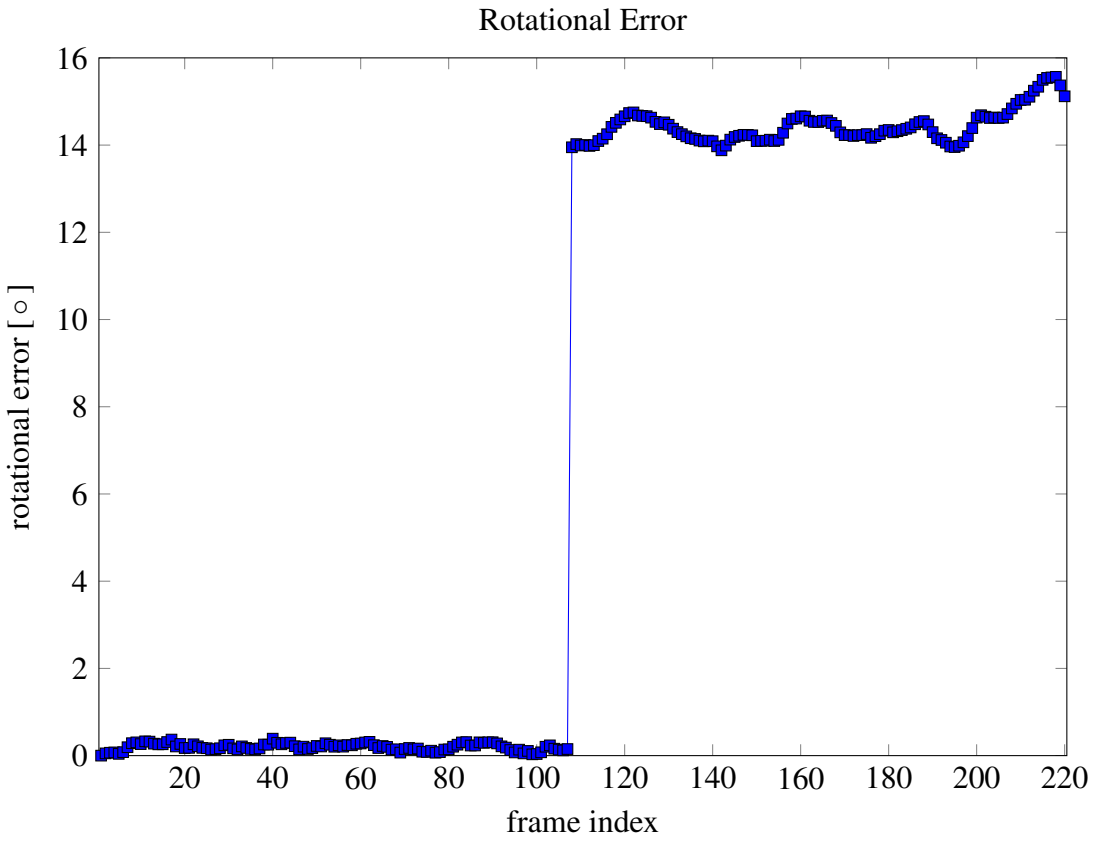
Rotational Error
rotational error [∘]
frame index
0
2
4
6
8
10
12
14
16
20
40
60
80
100
120
140
160
180
200
220

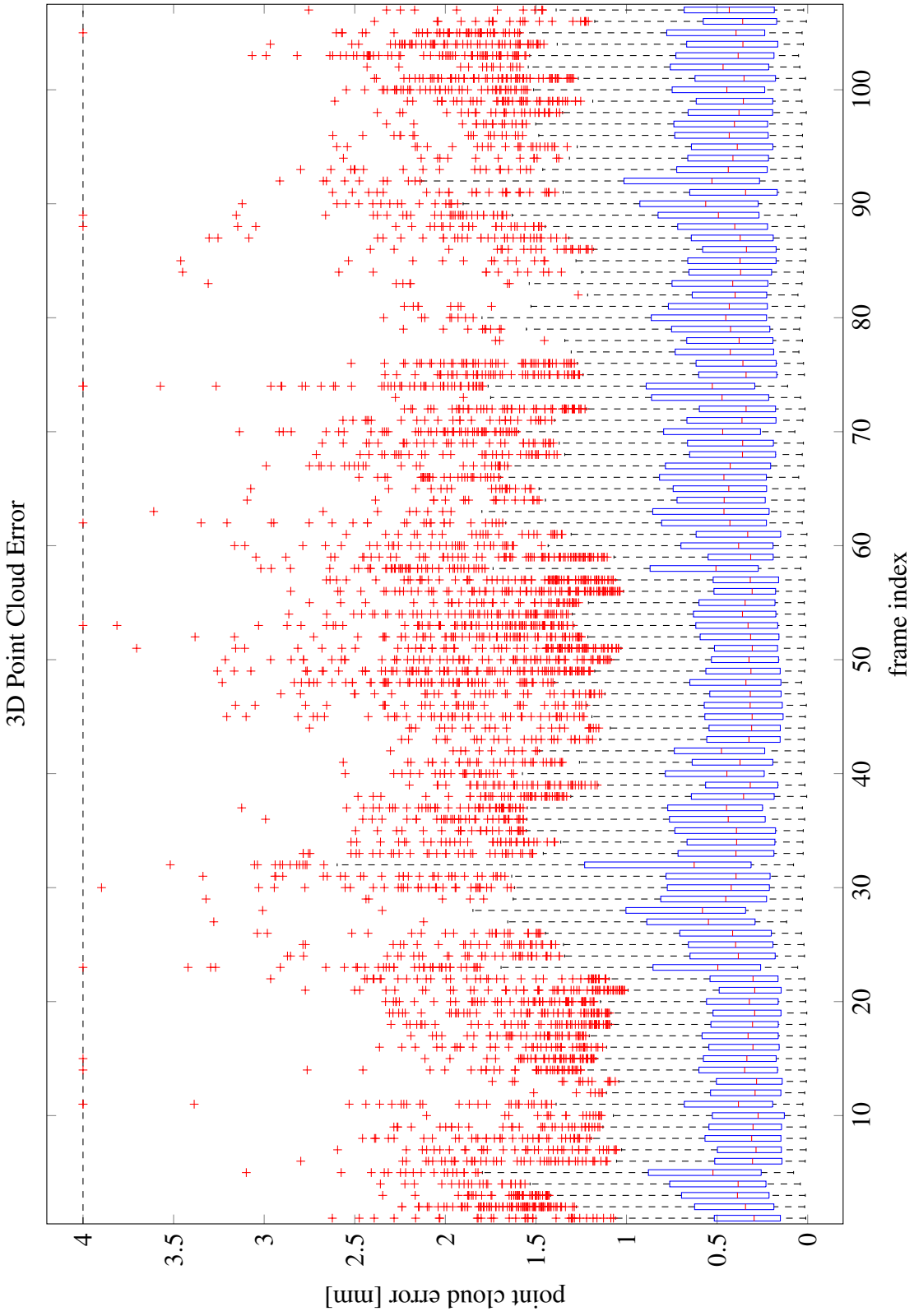

Figure C.12: Evaluation results of the sparse reconstruction of Phantom 3 Sequence 3.

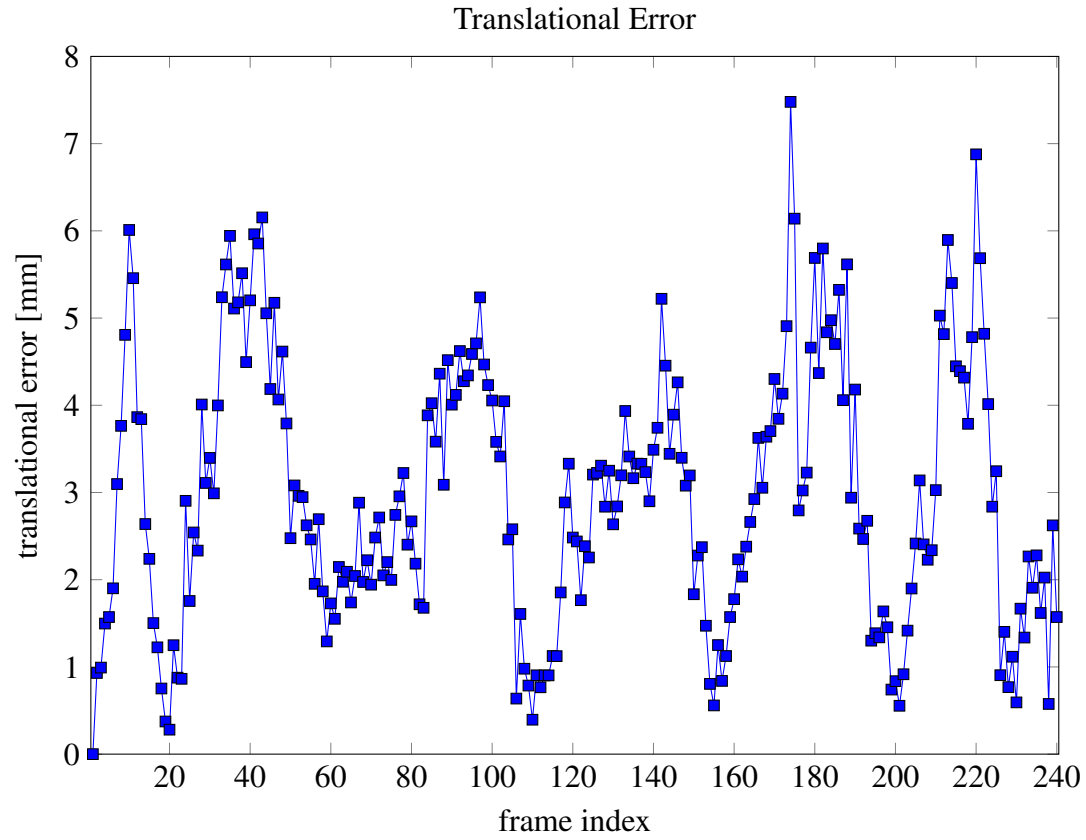
Translational Error
translational error [mm]
frame index
0
1
2
3
4
5
6
7
8
20
40
60
80
100
120
140
160
180
200
220
240

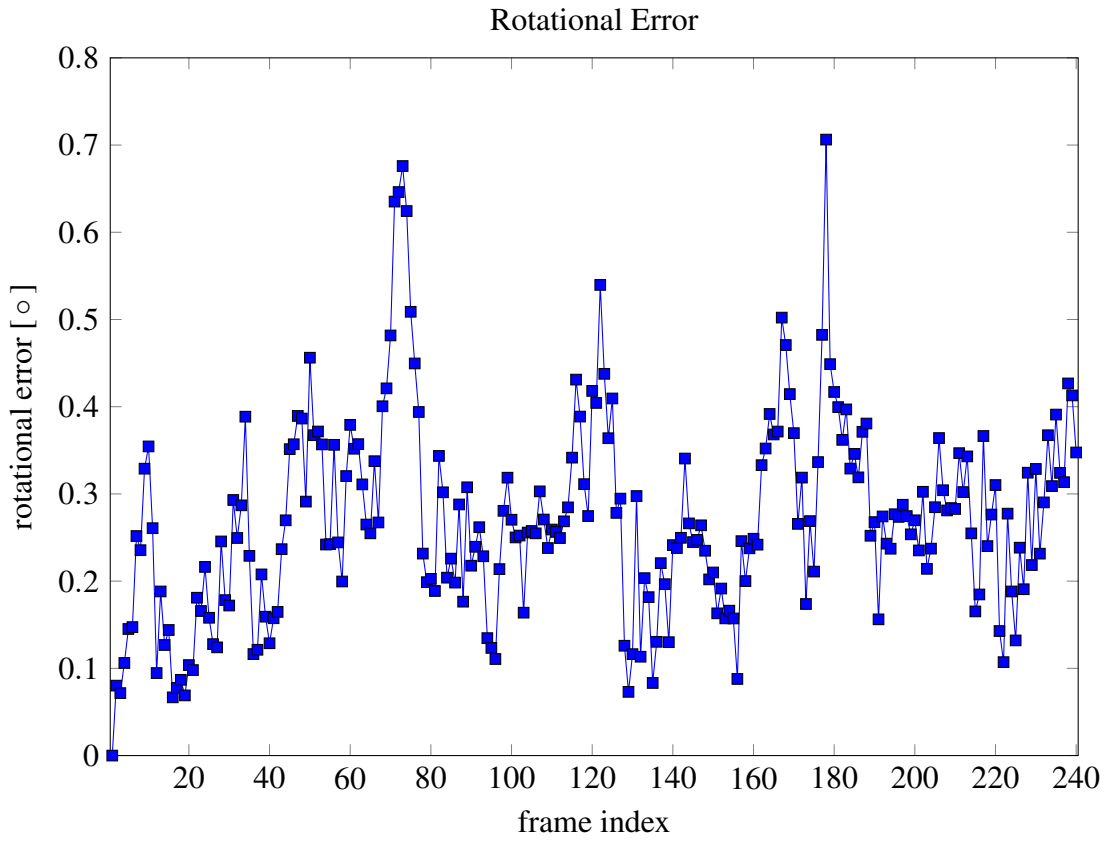
Rotational Error
rotational error [○]
frame index
0
0.1
0.2
0.3
0.4
0.5
0.6
0.7
0.8
20
40
60
80
100
120
140
160
180
200
220
240

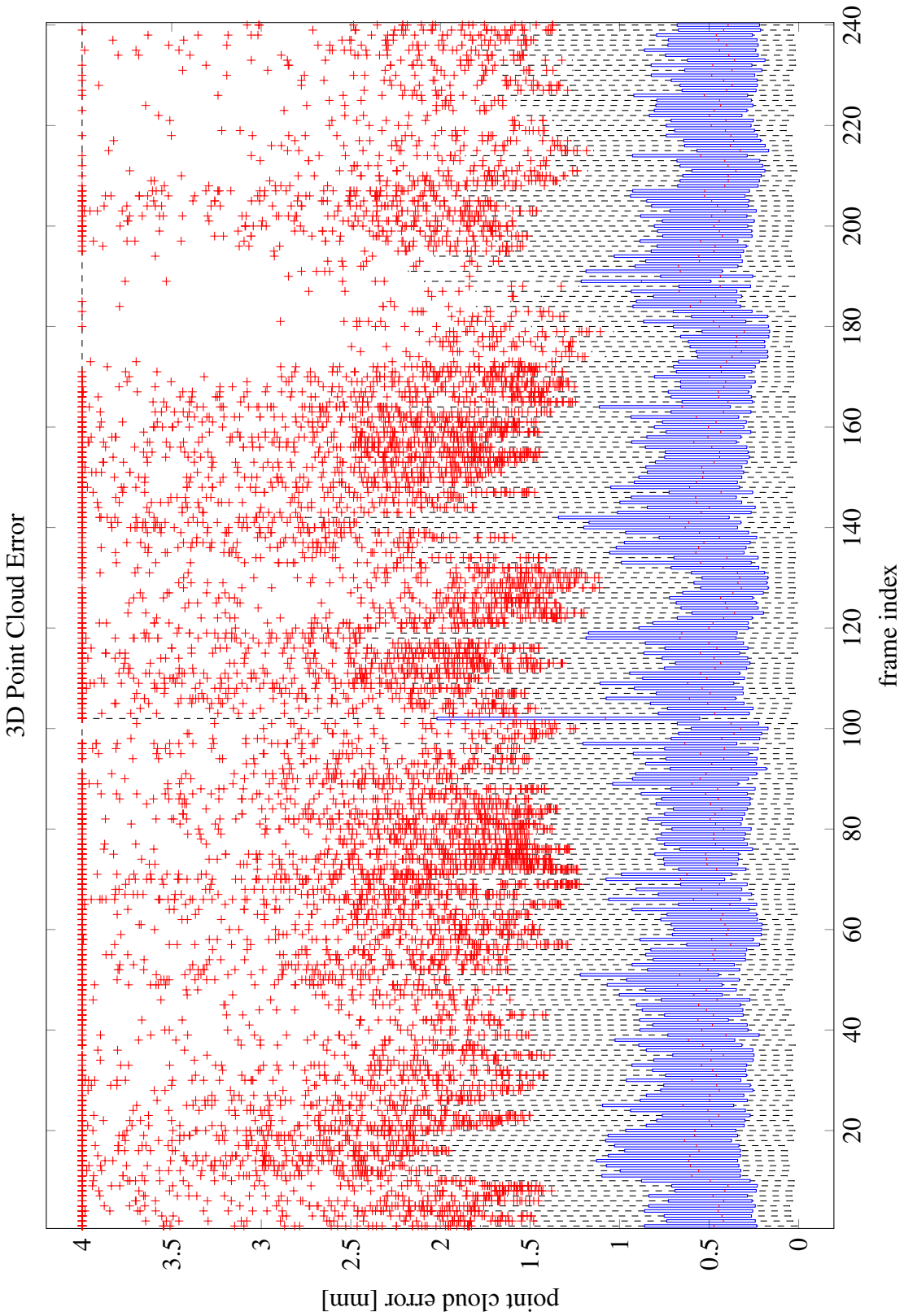

Figure C.13: Evaluation results of the sparse reconstruction of Phantom 3 Sequence 4.

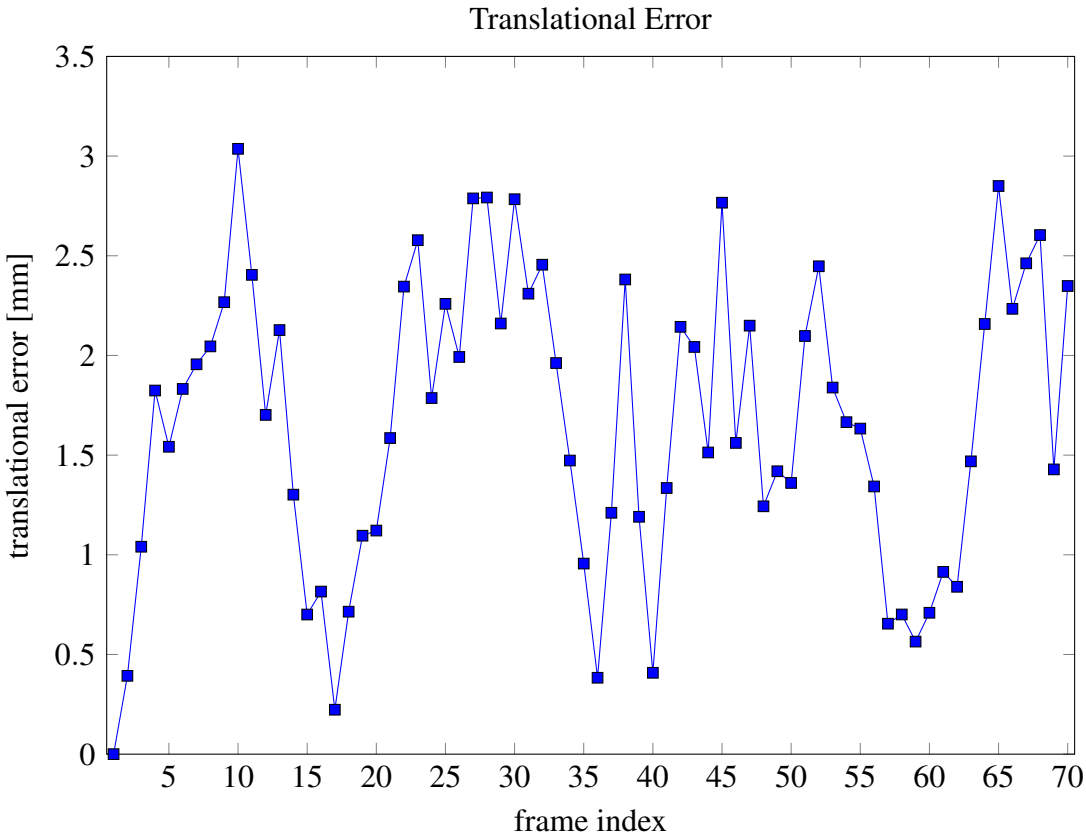
Translational Error
translational error [mm]
frame index
0
0.5
1
1.5
2
2.5
3
3.5
5
10
15
20
25
30
35
40
45
50
55
60
65
70

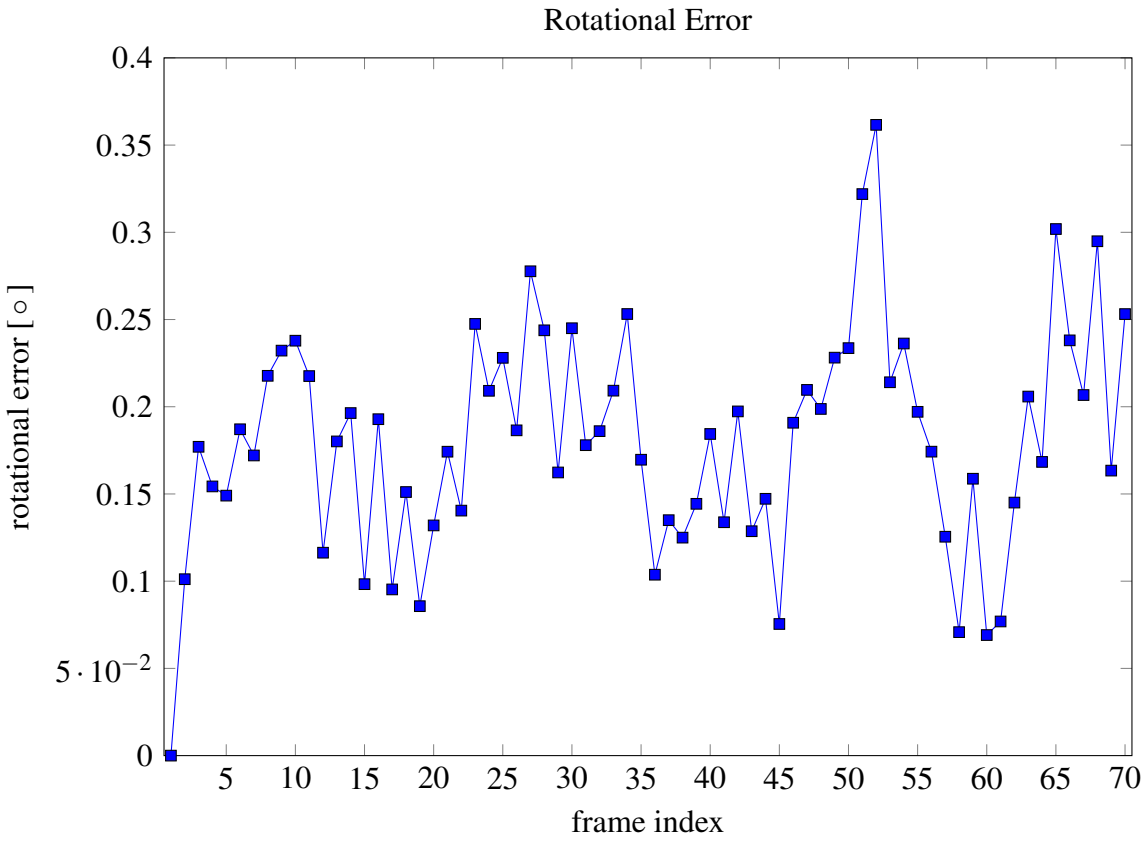
Rotational Error
rotational error [◦]
frame index
0
5 · 10−2
0.1
0.15
0.2
0.25
0.3
0.35
0.4
5
10
15
20
25
30
35
40
45
50
55
60
65
70

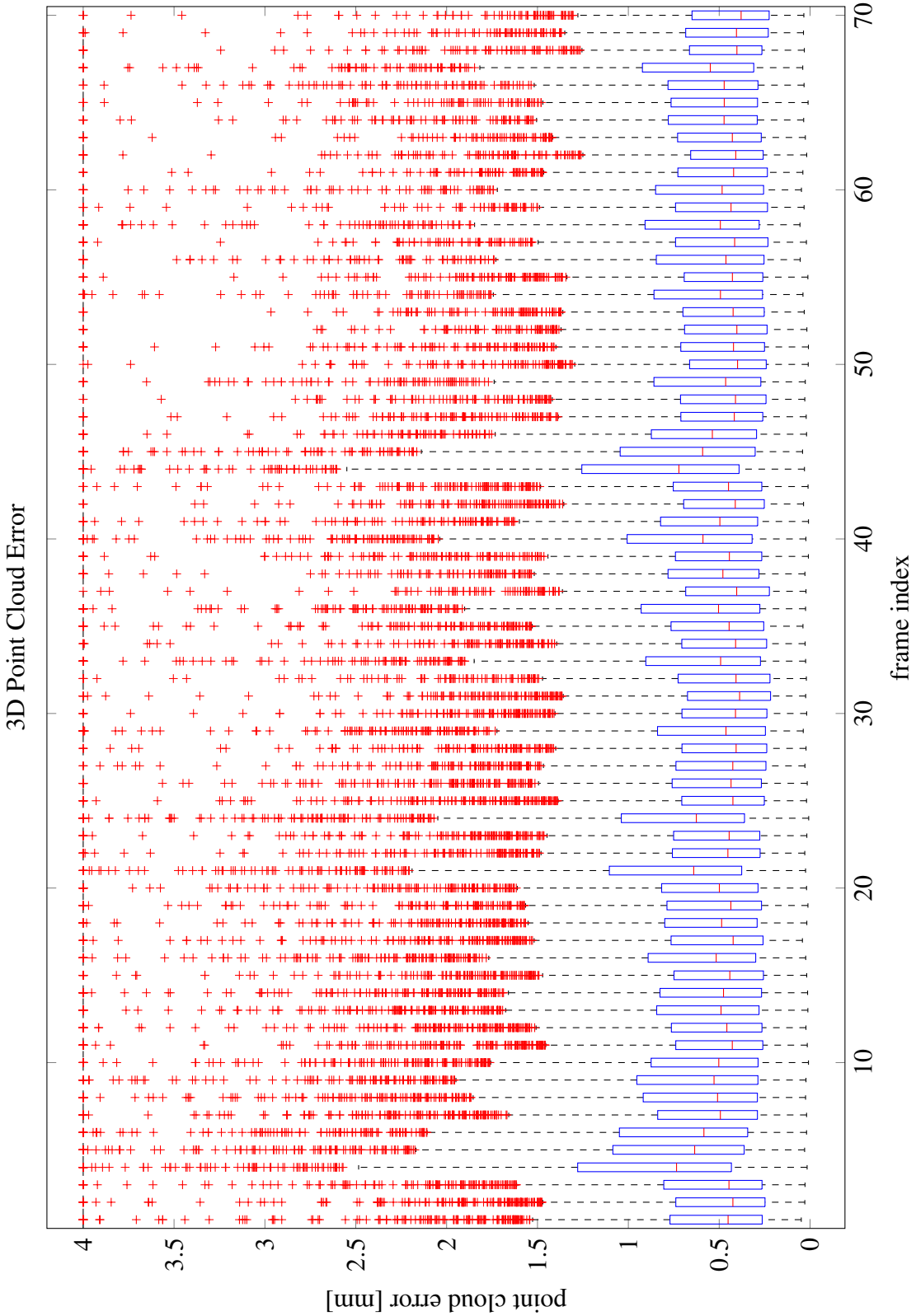

Figure C.14: Evaluation results of the sparse reconstruction of Phantom 3 Sequence 5.

Bibliography

[1] Jan Marek Marcinczak and Rolf-Rainer Grigat. Total Variation Based 3D Reconstruction from Monocular Laparoscopic Sequences. In *MICCAI 2014 Workshop on Abdominal Imaging: Computational and Clinical Applications*, volume 8676 of *Lecture Notes in Computer Science (LNCS)*. Springer, 2014.

Springer

http://www.springer.com/978-3-658-12697-1

Variation Based Dense 3D Reconstruction
Application on Monocular Mini-Laparoscopic Sequences

Painer, S.

2016, XV, 78 p. 34 illus., Softcover
ISBN: 978-3-658-12697-1